STRUCTURE AND EVOLUTION OF MODEL HELIUM STARS

Thesis by

Theodore Neil Divine

In Partial Fulfillment of the Requirements

For the Degree of

Doctor of Philosophy

California Institute of Technology

Pasadena, California

1965

(Submitted November 5, 1964)

PREFACE

This research was performed during the author's graduate study at the California Institute of Technology, where he was supported by a tuition scholarship and a research assistantship granted by the Institute, by the Air force Office of Scientific Research, and by fellowships awarded by Convair and by the National Science Foundation. The expenses of machine computation were met by the Division of Physics, Mathematics, and Astronomy of the California Institute, and by the Mount Wilson and Palomar Observatories. The author is indebted to Dr. J. B. Oke for suggesting and supervising the research, to Dr. Icko Iben, Jr., for frequent advice, and to numerous others for encouragement, discussion, and information in advance of publication.

List of correction in Theodore Neil Divine's thesis (1965)

Page	line (t=from top b=from bottom)	replace	with
16	t2	"decreases"	"increases"
19	b8	"(1964) stems"	"(1964) stem"
27	t8,9	"The were"	"The computations were"
33	b4	"oxclusively"	"exclusively"
35	b1	"Greenstein(1963)"	"Greenstein (1960)"
37	t9	"corsses"	"crosses"
37	b8	"then"	"them"
38	t9	"greated"	"greater"
45	eq. A33	$\left[1+\frac{\epsilon U}{2}\right]$	$\left[1+\frac{\epsilon U}{2}\right]^{3/2}$
108	b2	"3,0"	"3.4"

Note: these corrections have been made on the library copy of the thesis.

ABSTRACT

Numerical models have been constructed which describe the evolution of stars which are initially pure helium. The iterative technique, programmed for a large computer, permits the inclusion of radiation pressure, electron degeneracy, electron scattering opacity, gravitational contraction, and detailed composition changing brought about by triple-alpha and (α,γ) reactions.

The twenty homogeneous (pure helium) models, which range in mass from 0.4 to 60 $M_\odot$, form a "main sequence" on the left of the H-R diagram. Evolutionary sequences of models at 0.5, 1, and 6 $M_\odot$ exhaust their central helium supply in times of 80, 12, and 0.8 million years. Thereafter the convective core models, which have remained near their main sequence positions, are replaced by shell source models of increasing luminosity. At all three masses the final composition of the helium-exhausted core is almost exclusively oxygen, although a reduced rate for $C^{12}(\alpha,\gamma)O^{16}$ can lead to moderate fractions of carbon.

There is no clear indication that the models correspond to any group of observed stars. Massive helium star models may resemble Wolf-Rayet stars in mass, luminosity, and effective temperature.

TABLE OF CONTENTS

Title page i

Preface ii

Abstract iii

Table of Contents iv

PART I. INTRODUCTION 1

I-1. Background
I-2. Structural Assumptions
I-3. Structural Equations
I-4. Physical Assumptions
I-5. Computational Methods

PART II. HOMOGENEOUS HELIUM STARS 12

II-1. Homologous Models
II-2. The One Solar Mass Model
II-3. Main Sequence Models

PART III. EVOLUTION OF HELIUM STARS 20

III-1. Evolution at One Solar Mass
III-2. Evolution at Other Masses
III-3. Effect of a Reduced Reaction Rate

PART IV. CONCLUSION 29

IV-1. Internal Results
IV-2. External Results

APPENDIX A. PHYSICS OF THE STELLAR MATERIAL . . . 40

A-1. The Equation of State
A-2. Opacity
A-3. Nuclear Reactions

APPENDIX B. DETERMINATION OF A STELLAR MODEL . . . 57

B-1. The Trial Model
B-2. Iterations on the Trial Model
B-3. The Mass Level Structure

APPENDIX C. THE EVOLUTIONARY CALCULATIONS 68

C-1. Change in Chemical Composition
C-2. Gravitational Contraction
C-3. Time Step and Model Prediction

APPENDIX D. NOTATION 74

D-1. Intrinsic Quantities
D-2. Extrinsic Quantities
D-3. Constants

References 79

Tables 82

Figures 95

PART I. INTRODUCTION.

This introduction summarizes information essential to the research reported in the remaining parts. It first mentions the results of previous work on helium star models. Next are presented the assumptions of stellar structure by which this work is governed. A third section reviews the equations and boundary conditions which relate the variables throughout the star. The fourth section outlines the physics which relates the intrinsic variables at each point within the star. The fifth and last section mentions the computational techniques essential to the creation of the numerical stellar models.

Section I-1. Background.

Introductory to the work reported here is a glance at the published work of other authors. Models for homogeneous helium stars were first constructed by Crawford (1953). His pioneering work has been followed by Oke (1961), Cox and Giuli (1961), and Van der Borght and Meggitt (1963), each of whom has reported the characteristics of one or more models of nearly pure helium stars. Among these works perhaps the clearest exposition of a justification for the construction of such models is provided by Cox and Giuli (1961). These three works and forthcoming papers by Cox and Salpeter (1964) and Deinzer and Salpeter (1964) indicate the major features of the "helium star main sequence", a series of models for homogeneous

stars composed of nearly pure helium at various masses.

The following statements describing the structure of such model stars are implied by the above-mentioned works. Helium burning reactions are confined to a central core, within which convection transports the energy generated away from the center. In an envelope surrounding this core radiation carries the energy to the surface, where it passes through a stellar atmosphere and is radiated into the surrounding empty space. As the models increase in mass an increasing fraction of the mass is found in the convective core. The physics which describes the stellar material is indicated by the ranges of temperatures and densities. Their central values are appropriate for the triple-alpha reaction of helium burning. Degeneracy of the electrons near the center is significant only for the stars of small mass, and radiation pressure increases in importance as larger masses are considered. The stellar material is practically completely ionized throughout all the models, indicating that electron scattering is the predominant source of opacity in all but the outermost layers.

Cox and Salpeter (1964) conclude that homogeneous helium-burning stars can exist at masses greater than about 0.33 $M_\odot$; an approximate upper mass limit to the main sequence may be guessed at 100 or 200 $M_\odot$. For this mass interval Table 1 indicates the order of magnitude of several important quantities. These approximate values are drawn from the works mentioned above.

Models describing the evolution of stars which are initially on the "helium star main sequence" are reported by Aller (1959), Hayashi, Hoshi, and Sugimoto (1962), Osaki (1963), and in forthcoming works by Cox and Salpeter (1964) and Deinzer and Salpeter (1964). A class project in 1962 at the California Institute of Technology also attempted to construct models describing the evolution at one solar mass. These models provided valuable guidance for the present study by permitting the anticipation (qualitatively and quantitatively) of the following developments. As the helium in the core is depleted the star brightens and then moves toward higher effective temperatures. The core ceases to be convective when its helium is exhausted; thereafter the core contributes to the luminosity by cooling and gravitational contraction. A shell source generating energy by helium burning moves outward, leaving helium-depleted layers beneath it; degeneracy in the core and radiation pressure in the envelope increase in importance; and, as the envelope expands, the model star brightens and then moves towards lower effective temperatures and surface gravities. The present study confirms these developments.

Section I-2. Structural Assumptions.

The several assumptions involved in the construction of the models of the present study are mentioned here. The presence of rotation, pulsation, tidal forces, or large scale magnetic fields could lead to complex distortions or internal velocity fields and

mixing. In spite of the fact that such phenomena can have important effects on stellar structure and evolution, they are neglected in order that the present computations may take advantage of the enormous simplifications afforded by the mechanical assumptions of spherical symmetry and hydrostatic equilibrium.

Several mechanisms permit the generation and transport of energy. The energy stores of a star are nuclear, thermal, and gravitational; from them energy may be released by nuclear reactions, cooling, and gravitational contraction, and only in the forms of thermal motions and radiation (not, for example, in the form of neutrinos, which are neglected throughout this work). The transport of energy through the material of the star is achieved in a situation of either (a) "convective equilibrium", in which thermal energy is carried physically by turbulent motions of the material, and in which uniformity of composition is consequential; or (b) "radiative equilibrium", in which energy is carried in the form of photons and/or by the conduction of degenerate electrons. In no case is thermal diffusion allowed to transport either energy or nuclear species. The choice between (a) and (b) is made to yield the less steep of the appropriate temperature gradients. It is assumed that a temperature gradient equal to the adiabatic suffices to transport the energy in a convective regime; this is violated if a convective region exists near the surface, where at least a mixing length theory should be included. The structure of the surface layers is approximated by that of a grey stellar atmosphere which is stable both

against convection and against the blowing off of material by the radiation pressure of the emergent flux. The stellar models of the present study are required to obey all of the foregoing assumptions.

Section I-3. Structural Equations.

This section reviews the variables, differential equations, and boundary conditions appropriate to the construction of stellar models satisfying the assumptions of the preceding section. Several works present more complete justification, derivation, and description of similar material; among such works Sections 5, 6, and 7 of Schwarzschild (1958) are exemplary.

Physical variables and their logarithms are used to describe the structure of the star. The symbols used to represent these variables, and their descriptions and units, are listed in Appendix D. Considering M (the mass interior to the sphere of radius r) and t (time) as the independent variables, the differential equations relating the dependent variables r, L, T, and P to M and t are four in number. They appear here in dimensionless form. The radius equation, equivalent to the definition of density, is

$$\frac{M}{r}\frac{dr}{dM} = \frac{M}{4\pi r^3 \rho} \quad . \tag{1.1}$$

The luminosity equation, describing the conservation of energy, is

$$\frac{M}{L_o}\frac{dL}{dM} = \frac{M}{L_o}\left(\varepsilon - \frac{du}{dt} - P\frac{d}{dt}\left[\frac{1}{\rho}\right]\right) \quad . \tag{1.2}$$

The derivatives with respect to M and t are to be interpreted as partial derivatives to be taken holding the other independent variable constant. The temperature equations imply radiative transport

$$\frac{M}{T}\frac{dT}{dM} = -\frac{3\kappa}{4acT^4}\frac{ML}{16\pi^2 r^4} \tag{1.3}$$

or convective transport

$$\frac{M}{T}\frac{dT}{dM} = -\frac{\Gamma_2 - 1}{\Gamma_2}\frac{GM^2}{4\pi r^4 P} \quad . \tag{1.4}$$

The physics of stability against convection demands that, of the two equations, the one which yields the less negative value of the derivative be chosen. If we define the convection parameter by

$$\psi = \frac{16\pi acG}{3}\frac{MT^4}{\kappa LP} - \frac{\Gamma_2}{\Gamma_2 - 1} \tag{1.5}$$

an equivalent statement is that radiative transport prevails if ψ is positive, and convection occurs if ψ is negative. The pressure equation, describing material in hydrostatic equilibrium, is

$$\frac{M}{P}\frac{dP}{dM} = -\frac{GM^2}{4\pi r^4 P} \quad . \tag{1.6}$$

Let $\mathcal{M}$ denote the total mass of the model star (although the mass of the sun is denoted by $M_\odot$). The substitute independent variable $m = (\mathcal{M} - M)$ is useful in the region $M > (0.5)\mathcal{M}$, for which alternate forms of the above equations may be derived.

The differential equations permit the determination of stellar structure only when supplemented by appropriate boundary conditions. Analytic developments in the neighborhoods of the boundaries are

more convenient for numerical work. The surface is represented by $M = \mathcal{M}$ or by $m = 0$; near it the theory of stellar atmospheres provides such a development. We choose the simple case of a grey atmosphere, for which the descriptive equations are

$$P = \frac{GMm}{4\pi r^4} \tag{1.7}$$

and, adopting Eddington's approximate solution,

$$\frac{8\pi r^2 \sigma T^4}{L} = 1 + \frac{3}{2}\left[\tau = \frac{1}{4\pi r^2}\int_0^m \kappa dm\right] \quad . \tag{1.8}$$

The center is represented by $M = 0$; there the appropriate boundary conditions are $r = 0$ and $L = 0$. Let the subscript c denote values of the other physical variables at the center, and develop four quantities in powers of M near the center. The retention of the first terms in the developments for r and L yields

$$r = \left[\frac{3M}{4\pi\rho_c}\right]^{1/3} \tag{1.9}$$

and

$$L = M(\epsilon')_c \quad , \tag{1.10}$$

where, as everywhere in the star,

$$\epsilon' = \epsilon - \frac{du}{dt} - P\frac{d}{dt}\left[\frac{1}{\rho}\right] \quad . \tag{1.11}$$

Similarly the pressure and temperature developments yield

$$(P - P_c) = -\left[\frac{2\pi G\rho^2}{3}\right]_c \left[\frac{3M}{4\pi\rho_c}\right]^{2/3} \tag{1.12}$$

$$(T - T_c) = \begin{cases} -\left[\dfrac{\kappa\rho^2\epsilon'}{8acT^3}\right]_c \left[\dfrac{3M}{4\pi\rho_c}\right]^{2/3} \\ -\dfrac{\Gamma_2 - 1}{\Gamma_2}\left[\dfrac{2\pi G\rho^2 T}{3P}\right]_c \left[\dfrac{3M}{4\pi\rho_c}\right]^{2/3} \end{cases} \quad . \tag{1.13}$$

The choice between the radiative and convective forms of equation 1.13 must be made to yield the less negative value of $(T-T_c)$.

Section I-4. Physical Assumptions.

Accessory to the structural equations of the previous section are the constitutive relations among the intrinsic variables. The values of the constants required in these relations are taken largely from Allen (1963) and are listed in Section D-3.

The equation of state relates the density ρ, the internal energy u, and the adiabatic temperature gradient $\frac{\Gamma_2}{\Gamma_2-1}$ to the temperature T, the pressure P, and the chemical composition. The effects of radiation pressure, ionization of helium, and semi-relativistic, partially degenerate electrons cause the equation of state relations to differ from the basic perfect gas formula. In the calculation of the present models each effect is included only when the difference between its inclusion and its omission amounts to more than 10^{-4} in any quantity. The first section of Appendix A presents the required equations.

The opacity κ is a function of T, ρ, and the composition. Its major contributor is electron scattering; ionic sources of opacity (free-free transitions, bound-free transitions, and line absorption) are important near the surface; and conduction by degenerate electrons, when significant near the center, is included in the calculation of κ. The opacities used are obtained from

tabular material made available by A. N. Cox (1964) in advance of publication, and described briefly in Section A-2.

The reactions listed in Table 12 lead to nuclear energy generation. Helium-burning includes the triple-alpha and (α,γ) reactions which produce carbon, oxygen, and neon nuclei. The schematic carbon and oxygen burning reactions convert those nuclei into ones having atomic weights between 20 and 40. Throughout the computations the temperatures remained too low for these latter reactions to occur significantly. The details of the energy generation, and formulae for the computation of ϵ from T, ρ, and the composition, are discussed in Section A-3. The contributions of cooling and gravitational contraction to the energy release rate are included in equation 1.2.

Section I-5. Computational Methods.

The techniques used to construct the model stellar interiors resemble those suggested by Henyey et al. (1964), although several modifications of Henyey's method are employed. A particular value of the interior mass M characterizes each of several discrete mass levels. At each such level the computations must yield numerical values of the dependent variables r, L, T, and P and of the auxiliary variables ρ, κ, and ϵ. These eight variables, all evaluated at the same set of radially ordered points within the star, must be related in a way that satisfies simultaneously the equations of Section I-3

and the physics of Section I-4. The initial trial model, obtained from previous work, specifies values for the variables; usually the equations are not satisfied by this model. One then considers small changes in the values of the trial model, and requires that these changes permit the model to more closely satisfy the equations. This requirement leads to a complete set of equations linear in the changes; values for the changes may then be obtained by a specialized matrix inversion scheme. Applying the changes to the values of the trial model yields a new trial model. A few such iterations suffice to produce a model which satisfies the original relations to some required precision.

The creation of a satisfactory model at some particular time t_a is normally followed by the creation of a model at a later time t_b. The trial model at the new time is obtained by a linear extrapolation of the values of the dependent variables from the two (or, sometimes, one) previous models. As each iteration on the new model is performed the new composition is obtained from the former composition by the integration of the appropriate equations, schematically represented by

$$\frac{dx_A}{dt} = f_A(\rho, T, x_A,) \qquad (1.14)$$

at each mass level or within each convective region. In equation 1.14, x_A represents the fraction by mass of the nuclear species with atomic weight A, and x_A, implies that all the composition parameters may be required as arguments of f_A. The forms of the functions f_A are detailed in Section C-1. In addition, the new model must be

related to the former model in a way which satisfies equation 1.2. Appendices B and C present a detailed description of the method, including many necessary numerical techniques, as it is applied to the creation of both the homogeneous and evolved stellar models.

Both the number of values which must be easily accessible and the complexity of the numerical operations demand that a large electronic computer be used in order that the method be an economical one. The models were calculated by an IBM 7094 computer, supplemented by several specialized auxiliary machines. The program, written in FORTRAN IV, called for the use of most of the computer's 32,000 word memory; it permitted a maximum of 200 mass levels for a particular stellar model. The storage of previously computed models on magnetic tape was a standard procedure; for the models reported herein more detailed information may be obtained from a read-out of the models stored on tape.

Although cgs units are employed throughout the calculations, many of the results are quoted with reference to the sun. The values used for the sun, taken from Allen (1963), are listed in Section D-3.

PART II. HOMOGENEOUS HELIUM STARS.

The techniques outlined in Section I-5 and detailed in Appendix B have been used to create several numerical models for homogeneous helium stars. These models are characterized by the following composition parameters, specifying fractions by mass of the various constituents:

$$X = 0.000000 \qquad \text{(no hydrogen)}$$

$$Y = 0.999000 = x_{\alpha} \qquad \text{(helium, } He^{4}\text{)}$$

$$Z = 0.001000 \begin{cases} x_{12} = 0.000141 & \text{(carbon, } C^{12}\text{)} \\ x_{16} = 0.000420 & \text{(oxygen, } O^{16}\text{)} \\ x_{20} = 0.000298 & \text{(neon, } Ne^{20}\text{)} \\ x_{z} = 0.000141 & \text{(metals, A>20)} \end{cases}$$

The content of elements heavier than helium is similar to that of extreme Population II stars, and is responsible for the departure of the opacity values from those which would be derived for a pure helium composition.

An understanding of the models which will follow can be enhanced by the consideration of homology transformations among stellar models. Accordingly the first section briefly presents homology relations. The second section discusses the homogeneous helium star model at one solar mass. The third section presents the "helium star main sequence", a series of models which share the above composition and have various masses.

Section II-1. Homologous Models.

We first cast the constitutive relations in the following schematic forms:

state $\rho = \mu P/T^{\alpha}$ (2.1)

opacity $\varkappa = \text{constant}$ (2.2)

energy generation $\epsilon = x^3 \mu^2 \rho^2 T^{\nu}$. (2.3)

Here μ is to be interpreted as a quantity proportional to the molecular weight of the stellar material, and the exponent

$$\alpha = -\left[\frac{\partial \log \rho}{\partial \log T}\right]_P \quad . \tag{2.4}$$

Then equation 2.1 represents a degenerate gas law when α is small (less than unity), a perfect gas law when $\alpha = 1$, and a gas law including radiation pressure when α is large (greater than unity). Similarly the exponent

$$\nu = +\left[\frac{\partial \log \epsilon}{\partial \log T}\right]_P \tag{2.5}$$

permits equation 2.3 to represent nuclear energy generation. In the case of the triple-alpha reaction x may be taken as a quantity proportional to the fraction by mass of He^4, and 30 is a representative value for ν.

Those considerations required for the derivation of a homology transformation from the equations of the stellar interior have been applied using the schematic relations of equations 2.1

through 2.3. Let T, P, and x represent central values, μ and $\varkappa$ represent mean values, and M, R, and L represent surface values of the appropriate quantities. The proportionalities of the homology transaformation are then

$$T^{(\nu-4+12\alpha)} \propto \mu^{10} M^{6} / \varkappa x^{3} \qquad (2.6)$$

$$P \propto T^{4\alpha} / \mu^{4} M^{2} \qquad (2.7)$$

$$R \propto \mu M / T^{\alpha} \qquad (2.8)$$

and

$$L \propto \mu^{4} M^{3} T^{4(1-\alpha)} / \varkappa \quad . \qquad (2.9)$$

An expression for the effective temperature may also be obtained in the form

$$T_e^{4} = L/4\pi R^{2} \propto \mu^{2} M T^{4-2\alpha} / \varkappa \quad . \qquad (2.10)$$

Equations 2.6 and 2.9 imply a mass-luminosity relation among homologous models exhibiting identical composition and values of μ, $\varkappa$, and x in the form

$$\frac{\partial \log L}{\partial \log M} = \frac{3\nu+12+12\alpha}{\nu-4+12\alpha} \quad . \qquad (2.11)$$

For such models the elimination of M and T among equations 2.6 through 2.10 leads to the relation

$$\log T_e = \text{constant} - \left(\frac{\nu+20}{3\nu+12+12\alpha}\right)\left(\frac{M_{bol}}{10}\right) \quad . \qquad (2.12)$$

This equation represents a line in the $(M_{bol}, \log T_e)$ plane.

Section II-2. The One Solar Mass Model.

A model for a homogeneous helium star of one solar mass was obtained first. The model reported by Oke (1961) was used as a trial model. Several iterations were required to produce from this a satisfactory model including the physics described in Section I-4 and Appendix A. The final model had 109 mass levels and an indication of its precision is given by the statement that the inequalities B40 through B42 were all satisfied for $q = 1 \times 10^{-5}$.

This model, at a mass of 1.989×10^{33} gm, exhibits the numerical values mentioned in this paragraph. The behaviors of its dependent variables are summarized in Table 2 and displayed by Figure 1. The central temperature and density are 1.324×10^{8} °K and 6.00×10^{3} gm/cm^3 respectively. Nuclear energy generation by the triple-alpha reaction occurs wholly within a convective core containing 0.264 of the star's mass and extending from the center to 0.237 of its radius. In the surrounding radiative envelope the opacity of electron scattering and atomic processes ranges from 0.2 cm^2/gm in the interior to nearly 5 cm^2/gm at the surface. The atmosphere is characterized by an effective temperature of 52,300 °K and a gravity of 7.86×10^{5} cm/sec^2. The external radius is 1.299×10^{10} cm, 0.187 times that of the sun, and the total emergent flux is 9.277×10^{35} ergs/sec, 230 times that of the sun, at an absolute bolometric magnitude of -1.184.

The importance of electron degeneracy is designated by reference to the density ratio Λ which is defined by equation A53. At

the center of the one solar mass model $A = 0.974$; A remains constant throughout the convective core and decreases outward in the envelope, being greater than 0.99 in the outer tenth of the star's mass. Radiation pressure is designated by the value of β, the ratio of the gas pressure to the total pressure. In the one solar mass model β equals 0.985 at the center, reaches a maximum of 0.994 at an interior mass fraction of 0.945, and falls to 0.914 near the surface. Ionization is effectively complete everywhere; even at the surface only 0.0012 of the electrons are bound. Clearly none of the possible departures from the equation of state of a perfect gas are very important, although they were included in most of the calculations.

The model reported by Oke (1961) is in very good agreement with the present model. Both are nearly homologous to the ten solar mass hydrogen star model of Kushwaha (1957). Contrasted with Oke's model, the lower luminosity of the present model stems from the slightly higher value of $\frac{\Gamma_2}{\Gamma_2-1} = 2.6$, rather than 2.5, used in the convective core, and from the slightly higher opacity. Oke's energy generation formula yields a value for ϵ at the center about 30 times smaller than the one used here; consequently the logarithm of the central temperature is smaller than his by 0.046. The remaining quantities (radius and pressure) differ accordingly (i.e., obeying the transformations of equations 2.6 through 2.9) by similarly small factors. Comparisons may be drawn between this model and models at one solar mass obtained by other authors at the reader's discretion.

Section II-3. Main Sequence Models.

The sequence of twenty models of homogeneous helium stars at various masses was computed using, in addition to the techniques described in Section I-5 and Appendix B, the following scheme. Given a converged model at a particular mass, the numerical value of the stellar mass was changed artificially by a small amount with each iteration, as approximate convergence was maintained. When the desired mass for some model was reached the mass was held constant as successive iterations converged to a satisfactory model. Fourteen models proceeding from one $M_\odot$ to greater masses and five to lesser masses were thus obtained without requiring construction by the programmer of individual trial models. Each model so obtained had of the order of 100 mass levels; and the remarks concerning the accuracy of the model at solar mass are applicable to each of the others.

Numerical values for these models are summarized in Table 3. Figure 2 displays the locus of the models in the $(M_{bol}, \log T_e)$ plane; the equation

$$\log T_e = 4.655 - (0.053)\, M_{bol} \qquad (2.13)$$

describes the major portion of this line. These star models have effective temperatures about four times those of their counterparts at the same luminosity on the normal dwarf main sequence, and the slope of their locus is slightly steeper. Figure 3 displays the mass-luminosity relation for these models; they are brighter than

normal dwarf stars of the same mass by factors between about four (at the high mass end) and about 200 (at low mass). Values for $\frac{d\log L}{d\log M}$ range between 1.4 and 4.7, respectively. The models of low mass exhibit no instabilities. For masses greater than thirty $M_\odot$ the margin by which the force of gravity exceeds that of the emergent flux on the atmospheric layers is less than 25 % and a small change in the opacity or some other perturbation could subject the star to mass loss. Instability against pulsation could be responsible for an upper mass limit to the helium star main sequence.

Variations with mass of the central temperature, pressure, and density, and of the external radius and luminosity may be compared with the predictions of the homology relations of Section II-1. For neighboring models the predicted proportionalities are quantitatively correct if appropriate values of the exponents α and ν are employed. Electron degeneracy and conduction are more important in the models of small mass; $\Lambda = 0.85$ at the center of the $0.4\ M_\odot$ model. For masses greater than $3\ M_\odot$ degeneracy calculations were omitted. Radiation pressure was included in the calculations at all masses. It is most important in the more massive models; at $60\ M_\odot$ β ranges between 0.10 and 0.39. In addition it is primarily responsible for the marked increase with mass of the mass fraction q_f to be found in the convective core, whose boundary is fixed by the vanishing of ψ (cf. equation 1.5). The first term in ψ increases with increasing interior mass fraction; its variation is roughly the same for all the models of the main sequence. The second term in ψ varies with

β, the gas pressure fraction, as indicated in the last paragraph of Section A-1. Thus as radiation pressure increases in importance with mass, a greater fraction of that mass is included in the convective core. The numerical results of this effect appear in Table 3.

The results of the present study agree well with those of other recent investigations. The minor quantitative differences, at a given mass $\mathcal{M}$, among T_c, P_c, R, and $\mathcal{L}$ are attributable to the slightly different state, opacity, and energy generation relations employed. The lower luminosities of the small mass models (compared with the models of Cox and Salpeter (1964) stems from the larger opacity used; the more massive models agree well in luminosity and radius. These models contain a smaller mass fraction in the convective core than do their predecessors. This fact reflects the sensitivity which the requirement that ψ vanish at the core boundary introduces into this important quantity. That the core mass fractions be correct in the initial main sequence models is important for the subsequent evolution.

PART III. EVOLUTION OF HELIUM STARS.

Four series of numerical models describing the evolution of helium stars have been created using the computational techniques of Appendix C. One such series of sequential models, that for a one solar mass helium star, is discussed in some detail. The second section outlines the similar evolutionary developments exhibited by model sequences at 0.5 $M_\odot$ and at 6 $M_\odot$. The last section indicates the effect of a reduced rate for the $C^{12}(\alpha,\gamma)O^{16}$ reaction on the evolution at one solar mass.

Section III-1. Evolution at One Solar Mass.

Sixty-nine models following the one reported by Section II-2 describe the evolution of a helium star of one solar mass. Some of the important properties of selected models of this sequence appear in Tables 5 and 6. The evolutionary tracks in the $(\log T_c, \log \rho_c)$ and $(M_{bol}, \log T_e)$ planes are displayed respectively in Figures 9 and 13. Figure 4 displays the development of the central and average compositions with time, and Figures 1 and 5 through 8 display the profiles of r/R, $L/\mathcal{L}$, $\log T$, and $\log \rho$ within the star at selected times.

Initially the homogeneous star model has the configuration described in Section II-2. The first phase of the evolution, through the twenty-first model, is characterized by the continuing presence of a convective core, which contains approximately a constant fraction (0.267) of the star's mass. Within this core the composition is

uniform, and the curves subscripted c in Figure 4 describe its variation with time. At first the triple-alpha reaction produces C^{12}, which is eventually depleted by the growing importance of the $C^{12}(\alpha,\gamma)O^{16}$ reaction. By the time the helium is exhausted, at 12.2×10^{6} years, the core contains O^{16} almost exclusively. The composition change introduces a discontinuity in the molecular weight and the density at the edge of the convective core, which increases from a factor 1.00 to 1.33. During this phase the temperature and density within the core exhibit a steady increase, whereas within the envelope the density decreases slightly and the temperature remains approximately constant. The star brightens by 0.67 magnitude, first doing so at nearly constant effective temperature and then moving towards higher T_e, as the radius passes through a maximum and then falls sharply to a minimum. The effects of both degeneracy and radiation pressure, although increasing, continue to be minor. The opacity and energy generation rate retain approximately their initial values, and gravitational contraction makes a minor contribution (about 0.5 %) to the luminosity.

As might be inferred from a comparison of Figures 1 and 5, the consideration of a sequence of homologous models may contribute to an understanding of the early evolutionary development. As the helium content of the convective core is depleted, approaching zero from unity, the star's mean molecular weight increases from 1.333 to 1.453. In the homology equations x and μ change appropriately.

Initially the increasing molecular weight is responsible for increases in R and $\mathcal{L}$, as T_c and T_e change less markedly. Beyond about model 8 the influence of decreasing x (cf. equation 2.6) causes T_c to increase more rapidly than before, such that R decreases and T_e increases perceptibly. Thus as R goes through a maximum the star traces out the portions of its tracks in Figures 9 and 13 between models 0 and 21. As x, which represents the helium content of the core, approaches zero the homology considerations become inapplicable and only an examination of the details of the evolutionary models can reveal the accompanying events.

When the helium content of the core falls to zero several significant changes in the star's structure occur. Nuclear reactions can no longer serve as a source of energy in the core; nevertheless a temperature gradient still exists there, and energy continues to flow outward. Consequently as the core gives up thermal energy and contracts the central temperature decreases, the temperature gradient diminishes, and the central density continues to rise. As the flux in the core decreases convection is replaced by radiative equilibrium as the mechanism of energy transport. The temperature at the edge of the helium-exhausted core has risen (in the earlier stages) enough to permit helium burning in a shell source there to supply most of the star's luminous energy. Some of this energy is absorbed by the outer layers, resulting in their expansion and increasing the star's radius. The luminosity and surface area increase as T_e remains

approximately constant. The events of this paragraph occur between models 21 and 34 of the computations and occupy a time interval between 12.2 and 13.1 million years in the life of the star, when the model structure displayed in Figure 6 is exemplary.

The remaining evolutionary phase, described by models 34 through 69 of these computations, occupies the time interval between 13.1 and 16.7 million years. At its beginning the temperature gradient in the core has been reduced sufficiently that the central temperature passes through a minimum and starts to increase again. The shell source in which helium burning makes the major contribution to the luminosity begins at the same time to move away from the former convective core boundary. Within this shell source the nuclear reactions follow a pattern similar to the one originally followed within the core, characterized by the buildup of C^{12} and its subsequent depletion, leading to a final composition almost completely O^{16}. Throughout this phase the shell source, as it turns out, remains at a nearly constant distance from the center of the star and contains in a region of significant nuclear energy generation typically 0.10 of the star's mass (this falls to 0.05 somewhat later). It moves toward larger interior masses as the evolution proceeds, leaving behind a contracting oxygen core of increasing mass. The core makes only a minor contribution to the luminosity of the star, falling from about 12 % at the start of this phase to about 5 % at its conclusion. Within this core the temperature and density increase with time. The ratio

of the temperature at the center to that at the edge of the core ranges between 1.2 and 2.0; and degeneracy increases markedly in importance at the center, where Λ reaches 0.56 in the last model.

Figures 7 and 8 display the structure of the star during this phase. Clearly as the shell source moves outward in mass the homology considerations are inapplicable, and an easy explanation of the various developments is not available. Among these developments is a very significant increase in the radius of the star. This is accompanied by increasing luminosity in such a way that the star passes through a maximum T_e and then moves upward and to the right in the $(M_{bol}, \log T_e)$ plane. As this takes place radiation pressure increases in importance, growing to as much as half of the total pressure. Eventually the surface layers become unstable against convection, and this event forced the termination of the evolutionary computations, as the program was not equipped with techniques suitable for the handling of convective surface layers.

The several paragraphs of this section are summarized by Table 5. Table 4 explains the letters used to designate the various events and developments of the evolution.

Section III-2. Evolution at Other Masses.

The fifty-four sequential models describing the evolution at 0.5 $M_\odot$ and the fifty models describing the evolution at 6 $M_\odot$ are the subjects of this section. The major developments in the histories of these stars parallel the events discussed in the previous section for the one solar mass star; they are summarized in Tables 7 and 9.

The evolutionary tracks for the one half solar mass model are displayed in Figures 9 and 13; the development of the composition is shown in Figure 10; and the numerical values of important quantities for selected models are assembled in Table 8. Initially the homogeneous star has a convective core containing 0.224 of the star's mass. At the center the degeneracy indicator Λ equals 0.91, and radiation pressure is everywhere negligible. In the first stages of the evolution the central density decreases slightly (about 2 %); thereafter most quantities vary nearly as they do in the one solar mass case. At a time of 79×10^6 years the luminosity has risen 0.47 magnitude and the convective core has achieved its final composition of almost completely O^{16}. The following interval, to 84×10^6 years, is characterized by a radiative oxygen core whose central temperature drops sharply to a value almost as low as the initial central temperature, as the core gives up some of its thermal energy. Meanwhile the luminosity declines briefly, then rises another 0.33 magnitude. As the shell source moves away from the former core boundary the

central temperature climbs slowly. The luminosity grows and the star remains at approximately constant radius, as there does not seem to be enough energy available for its expansion. The computations were terminated after the fifty-fourth model, and at a time of 131.39×10^6 years, when an anomalous composition appeared. The time steps between the last few models were perhaps a bit too large, and there is some doubt about the validity of the computational results beyond about 120×10^6 years. The last reliable model displays a core containing about half of the star's mass as oxygen; at the center electron degeneracy reduces Λ to 0.49, and radiation pressure is everywhere insignificant.

The evolutionary tracks for the six solar mass model are displayed in Figures 9 and 13; the development of the composition is shown in Figure 11; and the numerical values of important quantities for selected models are assembled in Table 10. Initially the homogeneous star has a convective core containing 0.527 of the star's mass; degeneracy is everywhere negligible and radiation pressure varies between 12 and 48 per cent of the total pressure. The first stages of the evolution resemble those of the one solar mass model. The convective core grows quickly to 0.578 of the star's mass and remains there until the core's helium content falls below 0.01 by mass at about 0.848×10^6 years. When helium burning ceases at the center the composition there is 0.06 Ne^{20} and 0.94 O^{16} by mass; the star's luminosity has increased about 0.6

magnitude. Two developments then occur which distinguish this star's evolution from that at one solar mass: gravitational contraction of the core, providing about ten per cent of the star's luminosity, is sufficient to prevent the central temperature from falling; and a convective region just outside the shell source includes about 0.12 of the star's mass. The star moves toward lower effective temperatures, as the star expands and the outer layers absorb some of the energy from the interior. The were terminated after the fiftieth model, at a time of 0.8599×10^6 years, and at an average helium content of 0.423 by mass. In the last model degeneracy is everywhere negligible and radiation pressure provides between 23 and 66 per cent of the total.

For helium stars of various masses one might expect the time in their evolution at which the convective core exhausts its supply of helium to be proportional to Mq_f/L . Such a proportionality is quantitatively verified (to within a few per cent) by the three detailed evolutionary tracks, and may therefore be used with confidence to predict characteristic times for the other models of the helium star main sequence.

Section III-3. Effect of a Reduced Reaction Rate.

As is pointed out in Section A-3, there is considerable uncertainty in the rate of the reaction $C^{12}(\alpha,\gamma)O^{16}$. In order to ascertain the effect on the evolution, a sequence of models at one solar mass was created in which this reaction rate was reduced by a factor ten from its standard value. The computations were carried through 19 models nearly to the exhaustion of the core helium content, at a time of approximately 10.55×10^6 years. Important times in the evolution of this model star are included in Table 5. The composition in the convective core followed the development displayed by Figure 12, and the final composition was 0.55 C^{12} and 0.45 O^{16} by mass. The evolutionary tracks in the ($\log T_c$, $\log \rho_c$) and (M_{bol}, $\log T_e$) planes are effectively indistinguishable from the ones obtained for the one solar mass model employing the standard reaction rates. The only significant difference is evidenced by the shorter evolutionary time for the models with the reduced rate. This reflects the fact that not as much energy is released by the burning of a given amount of helium to approximately equal quantities of C^{12} and O^{16} as is released when O^{16} is the only product. Thus if the star is to retain the same luminosity in the two cases it will complete the reactions in a shorter time in the former case.

PART IV. CONCLUSIONS.

The major result of this study is the presentation of the evolutionary models described in the foregoing sections. They are intended to provide more reliable models describing the evolution of helium stars than have heretofore been available. As such it is hoped that they parallel, although less extensively, some of the recent research, using similar techniques, leading to models which describe the evolution of hydrogen stars. Of the remaining two sections, the first contrasts the present models with their predecessors, and comments on their internal structure and composition. The last section mentions those links which the model stars may have with actual, observable astronomical objects.

Section IV-1. Internal Results.

The evolutionary tracks described by the fitted models of other investigators (cf. the last paragraph of Section I-1) are essentially similar to those described by the models of the present study. In particular the convective core models correspond quantitatively very well to those of the current study if adjustments are permitted which superpose the initial homogeneous models. In this phase of the evolution the only major difference is that the time for helium depletion in the core is longer in the present models than in any of their predecessors. This results not from the smaller luminosity (which, at a given mass, would yield a longer

time), nor from their less massive cores (which would shorten the time), but from the fact that the current models employ nuclear reaction rates which lead to the release of more energy per helium nucleus consumed than do their predecessors. For example, in the works of Aller (1959), Osaki (1963), and Hayashi (1962) the terminal core composition is exclusively C^{12}, rather than O^{16}, and their masses, in solar units, and core exhaustion times, in millions of years, are (1.0,6.5), (0.8,10.6), and (0.5,23) respectively. Completion of the reactions to oxygen nearly doubles the available energy, and therefore, at a given luminosity, the accompanying time as well. The composition resulting from helium burning is discussed in more detail later in this section.

The same three authors included in their evolutionary calculations a few shell source models which necessarily exhibit the following defects: (1) they have carbon cores rather than oxygen cores; (2) the cores are assumed to be isothermal, implying the omission of energy release by either cooling or gravitational contraction; and (3) the energy generation occurs only in an artificially thin shell source at the boundary of the core. In spite of these defects the models manage to represent moderately well the stages in which the helium-exhausted core grows. Their evolutionary sequences differ quantitatively, but not qualitatively, from those of the present study.

Radiation pressure and electron degeneracy both increase in importance with time in all four series of evolutionary models. Radiation pressure remains negligible in the 0.5 $M_\odot$ model, and appears to have no decisive effect on the evolution even at 6 $M_\odot$, where its presence is important to the model structure. Electron degeneracy has only a one per cent effect on the density at the center of the last model at six solar masses, whereas in the lighter models it reaches an effect of a factor of two on the density in the last computed stages of the evolution.

The composition of the evolving models, both in the convective core and in the shell source, depends primarily on the ratios of the rates of the nuclear reactions of helium burning listed in Table 12; it is determined in detail by the integration of equations C5 through C9. The standard reaction rates used in three of the computed evolutionary sequences lead to a final composition of the helium-exhausted core which is almost completely O^{16}, with some Ne^{20} created in the core of the six solar mass model. Among these standard rates, the formula used for the $C^{12}(\alpha,\gamma)O^{16}$ reaction corresponds to a reduced alpha-particle width $\theta_\alpha^2 = 0.78$. The rate of this reaction is somewhat uncertain; it is discussed by Fowler and Hoyle (1964). If at one solar mass this rate is reduced by a factor ten the final composition contains approximately equal amounts of carbon and oxygen. The composition results of the present model calculations may be reasonably compared with those of Deinzer and Salpeter (1964).

They associate with $\theta_\alpha^2 = 0.4$ a rate for the $C^{12}(\alpha,\gamma)O^{16}$ reaction which is 2.9 times smaller than the standard rate used in this work. These authors present a thorough discussion of the composition of the cores of helium-burning stars ranging through a broad spectrum of masses. Parallel developments occur in shell sources undergoing helium burning, for which the present study finds a final composition almost completely O^{16} at the lower masses. Thus as the shell source moves away from the former convective core boundary no noticeable inhomogeneity occurs in the chemical composition of the growing, helium-exhausted core.

It is well known that the nuclear reactions by which hydrogen is fused into helium in stellar interiors cannot play a dominant role in the evolution of stars having less than some limiting small mass. Kumar (1963) has created models for hydrogen stars of low mass, and he finds 0.08 $M_\odot$ as an approximate value for the mass limit. For such a model the central temperature cannot exceed about 3×10^6 °K, a temperature below which hydrogen-burning is negligible. Similarly Cox and Salpeter (1964) find that model helium stars less massive than 0.35 $M_\odot$ cannot achieve central temperatures high enough to sustain helium-burning reactions (greater than 1×10^8 °K). The effect of electron degeneracy on the equation of state is responsible for this phenomenon; the limiting small mass models exhibit values of Λ near 0.6 in the central regions. The closest approach of the main sequence models of the present study to this limit is at a mass of 0.4 $M_\odot$, for which $\Lambda = 0.85$ and $T = 1.1 \times 10^8$ °K at the center.

The evolution which might be anticipated for helium star models beyond the termination of the sequences reported here is subject to similar considerations. The evolutionary sequences at 0.5, 1.0, and 6.0 $M_\odot$ are terminated at central values of Λ and T of (0.49, 1.5×10^8 °K), (0.56, 3.6×10^8 °K), and (0.99, 3.9×10^8 °K) respectively. The nuclear reactions of carbon and oxygen burning might be expected to be the next set of reactions to occur. The minimal temperatures for the $(C^{12}+C^{12})$, $(C^{12}+O^{16})$, and $(O^{16}+O^{16})$ reactions are of the order of 6, 9, and 13 times 10^8 °K respectively. At all three masses, therefore, the central temperature will have to increase considerably before carbon and oxygen burning reactions occur. Probably in the 0.5 $M_\odot$ model the central temperature will be limited by the effects of electron degeneracy to values too low to support these reactions, and the model, after helium burning ceases, will contract towards a white dwarf configuration. The one solar mass model may be expected to have the same fate, with two qualifications. First, its mass approaches the upper limiting mass for white dwarfs, and relativistic effects on the degenerate equation of state may become important. Second, if the final core composition contains an appreciable fraction of carbon the $(C^{12}+C^{12})$ reactions may be ignited, as they occur at lower temperatures than the $(O^{16}+O^{16})$ reactions which would be the only ones available for an oxclusively oxygen core; thus the choice of a rate for $C^{12}(\alpha,\gamma)O^{16}$ in the present models may be decisive in the next evolutionary stage. The six solar mass model may achieve temperatures at which the oxygen-burning

reactions occur; the effects of neutrino energy loss (cf. Fowler and Hoyle (1964)) may become significant at such temperatures, although they are negligible at the end of the present model computations.

Section IV-2. External Results.

A star may conceivably come to exist on the helium star main sequence in one of two ways. It may be the remnant of a star which has proceeded through the hydrogen-burning stages and then shed its hydrogen exterior. A less probable alternative is that it came into being through the contraction of a helium-rich cloud, expelled perhaps from an earlier generation of stars. The characteristic evolutionary time for a helium star is that time spent near the main sequence position, as the helium in the central convective core is consumed (leaving primarily oxygen in its stead). For the three detailed model series considered, at 6, 1 and 0.5 solar masses, the characteristic times are 0.8, 12, and 80 million years respectively. Thereafter about one half of the characteristic time is spent as the star brightens and burns helium in a shell source. The tracks in the (M_{bol}, $\log T_e$) plane exhibited by the models are displayed in Figure 13. Further evolutionary developments have not been considered in detail, but they may presumably include mass loss, contraction, and either the onset of carbon and oxygen burning or cooling toward a degenerate white dwarf configuration.

For the range of effective temperatures ($4.5 < \log T_e < 5.2$) of the current models neither theoretical nor observational studies have satisfactorily described the spectral distribution of the emergent flux. Were such a distribution available the bolometric magnitude could be related to a magnitude in a region of the spectrum accessible to conventional astronomical observation. Using a black body approximation to this distribution, O'Dell (1963) has determined bolometric corrections for this range of effective temperatures, relating M_{bol} to the international photographic magnitude scale by $BC = M_{bol} - M_{pg}$. The application of his bolometric corrections places the models of the present study in the $(M_{pg}, \log T_e)$ plane of Figure 14. This figure may then be used to compare the models with observed astronomical objects.

The other entries in Figure 14 represent observed stars in a schematic way. Their positions include some of the effects of reddening, blanketing, transfers among color systems and effective temperatures, and methods of obtaining distance moduli. Such manipulation of the observations is necessary to position the objects in the plane of Figure 14. The sources of these data follow. The "normal dwarf main sequence" is that adopted by Allen (1963). The globular cluster diagram (M5) is from Arp (1962) and Sandage (1962). The Wolf-Rayet stars are discussed by many authors (see below) and they probably fall somewhere in the region labelled WR in the figure. Greenstein (1963) discusses several varieties of blue stars, among

which are old novae, SS Cygni stars, hot subdwarfs, and faint blue stars. These objects all fall to the left of the main sequence (of hydrogen stars), but do not appear in Figure 14 for lack of specific data. Figure 3 in the letter of Harman and Seaton (1964) supplied the information on the nuclei of planetary nebulae (to which the abbreviation NPN is given). The line representing the white dwarfs (WD) was provided by Greenstein (1965).

The evolving helium star models of the present study spend most of their helium-burning lifetimes close to their main sequence positions, and therefore in a relatively narrow band in the plane of Figure 14. Cox and Salpeter (1961) demonstrate that if the outer several per cent of the mass of a helium star is replaced by a hydrogen-rich envelope the point representing the model is moved at constant luminosity toward lower effective temperatures; in this way the entire region between the helium and hydrogen main sequences may be bridged by helium star models. It is possible, therefore, that such modified helium star models may be reasonable ones for many of the stars reported by Greenstein (1960). The method by which Cox and Salpeter (1961) obtain a model for HZ 44 is exemplary.

It seems likely that the models of the present study are not simply related to the horizontal branch stars of globular clusters. The effective temperatures of the bluest of these stars are not known, but they may extend as far to the left in Figure 14 as $\log T_e = 4.5$. This does not warrant a statement linking them with the helium star

models. The models are incapable also of explaining the rare, very blue globular cluster stars of high luminosity and (possibly) low mass, mentioned by Arp (1958) and discussed by Traving (1962). The interpretation of both of these varieties of globular cluster stars must await the construction of stellar models with rather different, and almost certainly inhomogeneous, internal constitutions.

Harman and Seaton's (1964) sequence of NPN falls in the region also occupied by the helium star models. In the plane of Figure 14 the NPN sequence corsses the helium star main sequence at a model mass of about 2 $M_{\odot}$. These models, to which hydrogen-rich envelopes may be added (in the manner of Cox and Salpeter (1961)), may be capable of representing the NPN which fall on or to the right of the helium star main sequence. Nevertheless this possible interpretation seems unlikely for the three reasons that (a) a mass of about 1.2 $M_{\odot}$ for the NPN has been conjectured (on kinematical grounds) by O'Dell (1963) and other authors; (b) the NPN cannot form a group of similar objects and at the same time be explained as helium stars, because some of then almost certainly fall considerably to the left of the helium star main sequence; and (c) the lifetimes and evolutionary paths suggested for the NPN by O'Dell (1963) and by Harman and Seaton (1964) seem quite reasonable and are not at all consistent with a helium star model interpretation. These authors surmise that the interiors of the NPN involve no nuclear burning of fuels as light as helium, and that the luminosity arises from contraction, preceding the white dwarf phase for which energy is released by cooling.

The Wolf-Rayet stars may indeed correspond to the more massive helium star models. The existence of an extended envelope and other structural complications makes difficult the assignation of an effective temperature to the WR stars. They may lie in the range between the 13,000 ^{o}K color temperature and the 100,000 ^{o}K ionization temperature mentioned by Underhill (1960); the brightness temperature of 52,000 ^{o}K suggested by Rublev (1963) may be representative. The same authors suggest absolute visual magnitudes between -2 and -5; helium star models at masses greated than ten $M_{\odot}$ have comparable values of M_{pg}. For example, the helium star model at ten solar masses, using O'Dell's bolometric correction scale, has $M_{pg} = -1.66$. If by the addition of a hydrogen-rich shell the effective temperature is reduced to 60,000 ^{o}K and the luminosity remains the same the result is $M_{pg} = -3.7$. Limber (1964) quotes results which place the mass of two Wolf-Rayet stars (V444 Cygni and CQ Cephei) near 10 $M_{\odot}$. On the basis of such considerations it is reasonable to state that WR stars and helium star models may exhibit comparable masses (ten suns), luminosities (10^5 suns), and temperatures (several tens of thousands ^{o}K).

It will be recalled that the models near the upper mass end of the sequence of helium stars exhibit small margins of surface layer stability; i.e., the force of gravity exceeds that of the emergent flux by only a small factor. Disturbances occasioned by rotation and/or a companion star could result in the ejection of matter from such a star, and in the presence of a configuration of

gas beyond the star's surface. Such considerations for massive helium stars may correspond to the forced rotational instability proposed by Limber (1964) as an interpretation of the observed spectral characteristics of Wolf-Rayet stars. Kuhi (1964) has obtained photoelectric scans of WR stars; these scans show no evidence of a hydrogen contribution to any of the emission lines, whose relative intensities are consistent with He II identifications. The predominance of helium in the spectra of these stars' outer layers lends support to their interpretation as helium stars. The evolution of a ten $M_{\odot}$ helium burning star has a characteristic time of the order of 5×10^5 years, a short time which could be related to the rarity of WR stars. The extremely high temperatures and luminosities, coupled with only moderately high mass, which are currently accorded to the Wolf-Rayet stars may therefore be consistent with their interpretation as helium burning stars.

The comparisons drawn between helium star models and actual, observed stars are at best tentative. Nevertheless the present study has indicated the major properties and evolutionary developments of imaginary stars composed of pure helium. The final composition of almost exclusively oxygen is perhaps the result of most interest. Continuation of the evolutionary computations beyond the termination of the model sequences of this work might also be instructive.

APPENDIX A. PHYSICS OF THE STELLAR MATERIAL.

This appendix presents information sufficient for the calculation of ρ, $\varkappa$, ϵ, u, and $\Gamma_2/(\Gamma_2-1)$ for particular values of the temperature T, the pressure P, and the composition parameters X_z. In addition are required values of the logarithmic derivatives of ρ, $\varkappa$, ϵ', and u with respect to T and P. The method used to obtain these derivatives is illustrated by an example:

(a) calculate ρ from T and P

(b) choosing a small Δ, calculate ρ' from T and $P' = (1+\Delta)P$

(c) evaluate the derivative using the form

$$\frac{\partial \log \rho}{\partial \log P} = \frac{P}{\rho}\left[\frac{\partial \rho}{\partial P}\right]_T \approx \frac{1}{\Delta}\left[\frac{\rho'}{\rho} - 1\right] \quad . \tag{A1}$$

The procedure of the example may be readily extended to the numerical calculation of the eight required logarithmic derivatives. In this work Δ was taken as 10^{-3}. This numerical procedure makes simple the inclusion of all the physics involved in the calculation of ρ, $\varkappa$, ϵ', and u in that of their derivatives as well. That physics is presented in the three sections of this appendix, of which the first deals with the equation of state, the second with the opacity, and the third with the nuclear reactions leading to energy generation.

Section A-1. The Equation of State.

Consider a system of mass M, consisting of an assembly of particles at uniform temperature T and pressure P, and in thermodynamic equilibrium with its surroundings. In this assembly let each chemical element, specified by its atomic number Z and its atomic weight A, contribute a fraction x_Z to the mass of the system. Then the number of atoms of element Z is given by

$$N_Z = \frac{x_Z M}{AH} \quad . \tag{A2}$$

Let the state of ionization of the element Z be such that on the average Z′ electrons have been freed by each atom. Then the total numbers of atoms and electrons in the assembly are given respectively by

$$N_a = \Sigma N_Z = \frac{M}{H} \Sigma \frac{x_Z}{A} \tag{A3}$$

and

$$N_e = \Sigma Z' N_Z = \frac{M}{H} \Sigma \frac{Z'}{A} x_Z \tag{A4}$$

where the sums are to be taken over the elements Z. Defining the molecular weights for the atomic and electronic portions of the system respectively as the number of amu per particle we have

$$\mu_a = \frac{M/H}{N_a} = \frac{1}{\Sigma x_Z/A} \tag{A5}$$

and

$$\mu_e = \frac{M/H}{N_e} = \frac{1}{\Sigma Z' x_Z/A} \quad . \tag{A6}$$

The equation of state relates the intrinsic quantities x_Z, T, P, ρ, and u (cf. Appendix D), making use of such intermediate quantities

as Z', μ_a, and μ_e. The introduction of the extrinsic quantities M, N, U, and V aids in the presentation of equation of state information.

Let the total volume occupied by the assembly be V. Its relation with the density

$$\rho = \frac{M}{V} = \mu_e H \frac{N_e}{V} \tag{A7}$$

leads immediately to the relations

$$N_a = \frac{M}{\mu_a H} = \frac{\rho V}{\mu_a H} \tag{A8}$$

and

$$N_e = \frac{M}{\mu_e H} = \frac{\rho V}{\mu_e H} \quad . \tag{A9}$$

The pressure is the sum of radiation and gas kinetic pressures

$$P = P_r + P_g \tag{A10}$$

where

$$P_g = P_a + P_e \quad . \tag{A11}$$

The energy in the assembly is the sum of kinetic (thermal) energies of the atoms and electrons, potential energy of ionization, and energy in the radiation field:

$$U = U_a + U_e + U_i + U_r \quad . \tag{A12}$$

We shall be interested in the energy per unit mass, $u = \frac{U}{M}$.

Sufficient information about the radiation field is provided by

$$P_r = \frac{a}{3} T^4 \tag{A13}$$

and by

$$U_r = aT^4 V \quad . \tag{A14}$$

The first of these equations specifies a lower limit to the total pressure for a system in thermodynamic equilibrium at temperature T.

In most situations encountered in stellar interiors the atoms (or ions) obey the perfect gas law:

$$P_a = N_a kT/V \tag{A15}$$

and

$$U_a = \frac{3}{2} N_a kT \quad . \tag{A16}$$

The ionization of the atoms is responsible for the presence of the N_e free electrons and for the total energy of ionization U_i. In the notation of Allen (1963) the Saha equation is

$$\log \frac{N_{r+1}}{N_r} P_e = -\frac{5040}{T} \chi_{r,r+1} + \frac{5}{2} \log T - 0.4772 + \log \frac{2U_{r+1}}{U_r} \quad . \tag{A17}$$

The simultaneous solution of such equations for each adjacent pair of ionization stages and for each element enables us to obtain the average number of free electrons Z' contributed by each element, and the energy

$$U_i = \Sigma U_z N_z = \frac{M}{H} \Sigma U_z x_z / A \quad . \tag{A18}$$

The average ionization energy for the element Z, U_z, may be approximated by

$$U_z = \sum_{r=0}^{r'-1} \chi_{r,r+1} + (Z' - r')\chi_{r',r'+1} \tag{A19}$$

where r' is the greatest integer less than or equal to Z'. The values of Z' and U_i so obtained are to be used in equations A4, A6, and A12. For complete ionization simply set Z' equal to Z.

The electrons must be described as an assembly obeying Fermi-Dirac statistics, and situations arise in which they are partially degenerate and semi-relativistic. Chandrasekhar (1939)

presents the three equations

$$N_e = \frac{8\pi V}{h^3} \int_0^\infty \frac{p^2\, dp}{e^{\alpha+E/kT}+1} \tag{A20}$$

$$U_e = \frac{8\pi V}{h^3} \int_0^\infty \frac{E\, p^2\, dp}{e^{\alpha+E/kT}+1} \tag{A21}$$

and

$$P_e V = \frac{8\pi V}{3h^3} \int_0^\infty \frac{p^3}{e^{\alpha+E/kT}+1} \frac{\partial E}{\partial p}\, dp \quad . \tag{A22}$$

The correct relativistic relations between p and E are

$$p^2 = \frac{E^2}{c^2} + 2Em \tag{A23}$$

and

$$pdp = \left[\frac{E}{c^2} + m\right] dE \quad . \tag{A24}$$

The definition $u = \frac{E}{kT}$ leads to the intermediate relations

$$p = \left[(2mkT)u\left(1 + \frac{u}{2}\frac{kT}{mc^2}\right)\right]^{1/2} \tag{A25}$$

$$pdp = (mkT)\left[1 + u\frac{kT}{mc^2}\right] du \tag{A26}$$

and

$$\frac{\partial E}{\partial p}\, dp = (kT)\, du \quad . \tag{A27}$$

Appropriate substitutions yield

$$N_e = \frac{8\pi V}{h^3}(2mkT)^{\frac{1}{2}}(mkT)\int_0^\infty \frac{\left[\left(1+\frac{u}{2}\frac{kT}{mc^2}\right)\left(1+u\frac{kT}{mc^2}\right)^2\right]^{\frac{1}{2}} u^{\frac{1}{2}}\, du}{e^{\alpha+u}+1} \tag{A28}$$

$$U_e = \frac{8\pi V}{h^3}(kT)(2mkT)^{\frac{1}{2}}(mkT)\int_0^\infty \frac{\left[\left(1+\frac{u}{2}\frac{kT}{mc^2}\right)\left(1+u\frac{kT}{mc^2}\right)^2\right]^{\frac{1}{2}} u^{3/2}\, du}{e^{\alpha+u}+1} \tag{A29}$$

and $$P_e V = \frac{8\pi V}{3h^3}(kT)(2mkT)^{3/2} \int_0^\infty \frac{\left[(u)\left(1+\frac{u}{2}\frac{kT}{mc^2}\right)\right]^{3/2} du}{e^{\alpha+u}+1} \quad . \qquad (A30)$$

We define $\epsilon = \frac{kT}{mc^2}$ and introduce the three integrals $I_N^{1/2}$, $I_U^{3/2}$, and $I_P^{3/2}$, whose arguments, not explicitly stated, are α and ϵ. The definitions are

$$I_N^{1/2} = \int_0^\infty \frac{u^{1/2}\,du}{e^{\alpha+u}+1}\left[1+\frac{5}{2}\epsilon u + 2\epsilon^2 u^2 + \frac{\epsilon^3 u^3}{2}\right]^{1/2}$$

$$= N_e\left[\frac{(h^2/2mkT)^{3/2}}{4\pi V}\right] \quad , \qquad (A31)$$

$$I_U^{3/2} = \int_0^\infty \frac{u^{3/2}\,du}{e^{\alpha+u}+1}\left[1+\frac{5}{2}\epsilon u + 2\epsilon^2 u^2 + \frac{\epsilon^3 u^3}{2}\right]^{1/2}$$

$$= \frac{U_e}{kT}\left[\frac{(h^2/2mkT)^{3/2}}{4\pi V}\right] \quad , \qquad (A32)$$

and $$I_P^{3/2} = \int_0^\infty \frac{u^{3/2}\,du}{e^{\alpha+u}+1}\left[1+\frac{\epsilon u}{2}\right]^{3/2}$$

$$= \frac{P_e V}{2kT/3}\left[\frac{(h^2/2mkT)^{3/2}}{4\pi V}\right] \quad . \qquad (A33)$$

Equations A7 and A31 lead to an expression for the density,

$$\rho = \frac{\mu_e H}{kT}(4\pi mkT)\left[\frac{2mkT}{h^2}\right]^{3/2} I_N^{1/2} \quad . \qquad (A34)$$

Equations A8, A11, A15, A33, and A34 lead to an expression for the gas pressure

$$P_g = P_e + \frac{\rho kT}{\mu_a H}$$

$$= (4\pi mkT)\left[\frac{2mkT}{h^2}\right]^{3/2}\left[\frac{2}{3}I_P^{3/2} + \frac{\mu_e}{\mu_a} I_N^{1/2}\right] \quad . \qquad (A35)$$

Lastly the internal energy is given by

$$\frac{U_a}{M} + \frac{U_e}{M} = \frac{\frac{3}{2} N_a kT}{\mu_a N_a H} + \frac{U_e}{\mu_e N_e H}$$

$$= \frac{3}{2} \frac{kT}{\mu_a H} \left[1 + \frac{\mu_a}{\mu_e} \frac{2}{3} \frac{I_U^{3/2}}{I_N^{1/2}} \right] \quad . \tag{A36}$$

The equations describing the behavior of the radiation, the atoms, and the electrons are all the analytic relations required for the equation of state calculations.

For the purposes of calculation the evaluation of the equation of state is divided into two cases: the degenerate case, in which a technique for the numerical evaluation of the three integrals is used; and the non-degenerate case, in which a perfect gas law, modified to include the first degenerate term, is used.

For the perfect gas case we consider the three integrals to be equal to the Fermi-Dirac functions F_s, which is equivalent to setting ϵ equal to zero. Thus

$$I_N^{1/2} = F_{1/2} \tag{A37}$$

and

$$I_U^{3/2} = I_P^{3/2} = F_{3/2} \quad . \tag{A38}$$

For small degeneracy it is well known that

$$F_s = \int_0^\infty \frac{u^s \, du}{e^{\alpha+u}+1} \approx e^{-\alpha} \Gamma(s+1) \left[1 - \frac{e^{-\alpha}}{2^{s+1}} + \cdots \right] \quad . \tag{A39}$$

This approximation leads to

$$\frac{\rho kT}{\mu H P_g} = 1 - \frac{\mu}{\mu_e} \frac{e^{-\alpha}}{4\sqrt{2}} \tag{A40}$$

and $$\frac{u_g}{\frac{3}{2} kT/\mu H} = 1 + \frac{\mu}{\mu_e} \frac{e^{-\alpha}}{4\sqrt{2}} \quad , \tag{A41}$$

where $$e^{-\alpha} = \frac{\mu}{\mu_e} \left[\frac{h^2}{2\pi m k T}\right]^{3/2} \frac{P_g}{2kT} \tag{A42}$$

and $$\mu = \frac{\mu_a \mu_e}{\mu_a + \mu_e} \quad . \tag{A43}$$

This perfect gas law including the first degenerate term is used in the model calculations whenever $e^{-\alpha}$ is less than 0.05. For the lower temperature range of this perfect gas region iterations among equations A6, simultaneous equations of the form A17 (yielding Z′), and the relation $P_e = P_g \mu/\mu_e$ are performed to obtain μ_e. Elsewhere complete ionization is assumed, yielding, for these compositions, $\mu_e = 2$.

For the degenerate case more complex techniques are required. Consider integrals of the form, involving the function f(u),

$$I_f^s = \int_0^\infty \frac{u^s \, du}{e^{\alpha+u} + 1} f(u) \quad . \tag{A44}$$

Approximating f(u) by

$$f(u) \approx 1 + \frac{u}{u_1} \left[f(u_1) - 1 \right] \quad , \tag{A45}$$

where u_1 remains arbitrary, an evaluation of I_f^s is

$$I_f^s \approx F_s + \left[\frac{f(u_1) - 1}{u_1} \right] F_{s+1} \quad . \tag{A46}$$

This approximate equality may be made exact for all functions f(u) of the form $(1 + au + bu^{3/2})$ by choosing

$$u_1 = \left[\frac{F_{s+3/2}}{F_{s+1}} \right]^2 \quad . \tag{A47}$$

With this choice the right-hand side of equation A46 evaluates I_f^s

(a) exactly for the non-relativistic degenerate case,

(b) to within about one per cent for the completely degenerate case ($|\alpha|$ large; as checked against the representation of Schwarzschild (1958), page 61),

(c) exactly for the very relativistic degenerate case (ϵ large), and

(d) exactly for the completely non-degenerate case (α large),

and is expected to be good to within five per cent in all intermediate regions.

The five Fermi-Dirac functions $F_{1/2}$, $F_{3/2}$, F_2, $F_{5/2}$, and F_3 are required for the evaluation of $I_N^{1/2}$, $I_U^{3/2}$, and $I_P^{3/2}$ via equations A46 and A47. Let the independent variable α be replaced by an alternate degeneracy parameter ν, chosen so that

$$\nu \approx \begin{cases} e^{-\alpha} & \text{for small } \nu, \text{ large } \alpha \\ \alpha^2 & \text{for large } \nu, \text{ large } (-\alpha) \end{cases} \quad . \tag{A48}$$

In this way the limiting behaviors of F_s

$$F_s \approx \begin{cases} \Gamma(s+1)e^{-\alpha} \approx \Gamma(s+1)\nu & \text{for small } \nu \\ \frac{1}{s+1} |\alpha|^{s+1} \approx \frac{1}{s+1} \nu^{(s+1)/2} & \text{for large } \nu \end{cases} \tag{A49}$$

involve no transcendental functions of ν. Let ν be defined by its relation to $F_{1/2}$

$$F_{1/2} = \frac{2}{3} \nu \frac{(2.6971154 + \nu)^{3/4}}{(1.5832098 + \nu)} \qquad (A50)$$

and evaluate the four remaining functions by the approximation formula

$$F_s = \frac{\nu}{s+1} \left[g_o + \nu \right]^{\frac{s+1}{2}} \left[\frac{a_o + a_1 \nu + \nu^2}{b_o + b_1 \nu + b_2 \nu^2 + \nu^3} \right] . \qquad (A51)$$

Appropriate choices of the five constants a_o, a_1, b_o, b_1, and b_2 for each of the functions F_s are listed in Table 11; they were obtained by requiring that equation A51 reproduce F_s exactly at the four points $\alpha = -1$, $+1$, $+3$, and $+6$ and that

$$\left[\frac{1}{s+1} \right] \frac{a_o}{b_o} (g_o)^{\frac{s+1}{2}} = \Gamma(s+1) \qquad (A52)$$

where $g_o = 2.6971154$ is the same for all values of s. The values to which the F_s were fitted have the following sources: for $F_{1/2}$ and $F_{3/2}$ they were obtained from McDougall and Stoner (1939); for F_2 and F_3 they were obtained from numerical integrations by Castor (1961); and for $F_{5/2}$ they were interpolated among the others. By comparing these tabulations with calculations using equation A51 it may be verified that the approximations yield values for the Fermi-Dirac functions accurate to better than 0.1 per cent.

For any given value of ν all five Fermi-Dirac functions can be evaluated numerically by performing only two square roots, five divisions, 30 multiplications, and several additions. Only a few

more operations, described by equations A46 and A47, are required in order to obtain $I_N^{1/2}$ and $I_P^{3/2}$, from which P_g is readily calculated via equation A35. A few iterations (changing ν) suffice to duplicate P_g to within 10^{-6}, and then ρ and u may be calculated using equations A34 and A36. An indication of the importance of degeneracy is given by

$$\Lambda = \frac{(\mu_a + \mu_e)\, I_N^{1/2}}{\mu_a \frac{2}{3} I_P^{3/2} + \mu_e I_N^{1/2}} \quad . \tag{A53}$$

Λ is the ratio of the correct density to the density which would be calculated for a completely ionized perfect gas of the same composition and at the same temperature and pressure.

In dense matter thermal conduction by degenerate electrons supplements radiation as a means of energy transport. Information sufficient for the calculation of the thermal conductivity is presented by Mestel (1950) and is amplified by A. N. Cox (1961). The conductivity ν_c is given by

$$\frac{1}{\nu_c} = \frac{10^{13}}{T^4}\frac{\rho}{\xi} \Sigma \frac{Z^2}{A} \left\{ - \ln \left[\sin \frac{1}{2} \left(\frac{1}{Z\zeta} \right)^{1/3} \right] \right\} \tag{A54}$$

where ζ and ξ are functions of the degeneracy parameter α. Their limiting behaviors, in terms of the alternate parameter ν, are

	$1/\zeta$	ξ	
for small ν:	$(0.5894)^3 \nu$	$128\, 10^{13} \frac{mk^5}{h^3 e^4 N_o} \nu = (6.2711)\nu$	(A55)
for large ν:	$(0.8475)^3$	$\frac{16\pi^2}{9} 10^{13} \frac{mk^5}{h^3 e^4 N_o} \nu^{3/2} = (0.80589)\nu^{3/2}$	(A56)

.

For intermediate values of ν Cox provides tables of $(1/\zeta)^{\frac{1}{3}}$ and ξe^{α} to which were fitted the following numerical approximations:

$$\text{for all } \nu: \quad \frac{1}{\zeta} = \nu \left[\frac{2.49492 + (0.60872)\nu}{12.1852 + (10.3873)\nu + \nu^2} \right] , \tag{A57}$$

$$\text{for } \nu \leq 30: \quad \xi = \nu \left[\frac{1119.31 + (379.370)\nu}{178.487 + (89.0681)\nu - \nu^2} \right] , \tag{A58}$$

$$\text{and for } \nu > 30: \quad \xi = \nu^{\frac{1}{2}} \left[\frac{4238.08 + (459.570)\nu + (0.80589)\nu^2}{515.544 + \nu} \right] . \tag{A59}$$

These approximations reproduce Cox's tables to within a few per cent and permit computation of the required conductivity via equation A54.

The last exercise in this section derives an expression for the adiabatic temperature gradient by returning to a consideration of the system of mass M, volume $V = \frac{M}{\rho}$, and internal energy $U = Mu$. Choose T and P as the independent variables and write the heat exchanged by the system with its surroundings in any quasi-static change:

$$\begin{aligned} dU + PdV &= Mdu - \frac{MP}{\rho^2} d\rho \\ &= M \left\{ \left[\frac{\partial u}{\partial T}\right]_P dT + \left[\frac{\partial u}{\partial P}\right]_T dP - \frac{P}{\rho^2}\left[\frac{\partial \rho}{\partial T}\right]_P dT - \frac{P}{\rho^2}\left[\frac{\partial \rho}{\partial P}\right]_T dP \right\} . \end{aligned} \tag{A60}$$

For an adiabatic change this heat vanishes, leading to the adiabatic temperature gradient:

$$\frac{\Gamma_2}{\Gamma_2 - 1} = \left\{ \frac{dP/P}{dT/T} \right\}_{ad} = \frac{\frac{T}{u}\left[\frac{\partial u}{\partial T}\right]_P - \frac{P}{\rho u}\frac{T}{\rho}\left[\frac{\partial \rho}{\partial T}\right]_P}{\frac{P}{\rho u}\frac{P}{\rho}\left[\frac{\partial \rho}{\partial P}\right]_T - \frac{P}{u}\left[\frac{\partial u}{\partial P}\right]_T} . \tag{A61}$$

The calculation of the logarithmic derivatives of ρ and u can be followed immediately by the calculation of $\Gamma_2/(\Gamma_2 - 1)$ via equation A61. This quantity is required for the consideration of convective equilibrium in the stellar interior (cf. Section I-3 and Appendix B). It may differ from 2.5 if the effects of ionization, radiation pressure, and semi-relativistic, partially degenerate electrons are included in the calculation of ρ and u.

If in such a calculation are included only a perfect gas with ratio of specific heats $\gamma = C_p/C_v$ and the effects of radiation pressure, equation A61 leads to

$$\left[\frac{\Gamma_2}{\Gamma_2 - 1}\right] = \frac{\beta^2 + (16 - 12\beta - 3\beta^2)(\gamma - 1)}{(4 - 3\beta)(\gamma - 1)} \quad . \qquad \text{(A62)}$$

For a perfect monatomic gas $\gamma = 5/3$ and $\Gamma_2/(\Gamma_2 - 1)$ ranges from 2.5 under conditions of negligible radiation pressure ($\beta = 1$) to 4 under conditions in which the gas pressure is small compared to the radiation pressure (β approaching zero).

Section A-2. Opacity.

The opacity was obtained by machine interpolation in a table of opacities supplied in advance of publication by A. N. Cox (1964). Where important the contributions of electron scattering, free-free transitions, bound-free transitions, and line absorption were included

in his calculated absorption coefficients. These formed the basis for integrations over frequency to yield Rosseland mean opacities, which were tabulated for discrete values of composition, temperature, and density. The two opacity tables used have the composition summaries and ranges indicated:

	first table	second table
x_H	0.000000	0.000000
x_α	0.999000	0.000000
x_{12}	0.000141	0.999000
x_{16}	0.000420	0.000488
x_{20}	0.000298	0.000347
x (others)	0.000141	0.000165
smallest (ρ,T)	$(10^{-10}$ gm/cm^3, 1.5×10^4 °K)	$(10^{-6}$ gm/cm^3, 10^6 °K)
largest (ρ,T)	$(10^{10}$ gm/cm^3, 10^9 °K)	$(10^{10}$ gm/cm^3, 10^9 °K)
total number of entries	144	80

When a numerical value for the opacity $\varkappa_R$ was required for some mass level, the machine searched the tables and, after finding the nearest tabular points, interpolated $\log \varkappa_R$ linearly in $\log \rho$, $\log T$, and x_α.

Where the conductivity of the degenerate electrons became important the material in Section A-1 was used to calculate ν_c. It was combined with $\varkappa_R$ to yield the effective opacity $\varkappa$ via the formula

$$\frac{1}{\varkappa} = \frac{3\rho\nu_c}{4acT^3} + \frac{1}{\varkappa_R} \quad . \tag{A63}$$

The numerical values of the opacity $\varkappa$ obtained by the techniques outlined in this section should be reliable to about twenty per cent.

Section A-3. Nuclear Reactions.

The nuclear reactions whose effects are included in these evolutionary models are summarized in Table 12. From particular values of the temperature and density the reaction rates R may be calculated independently of the composition, using material described by Fowler and Hoyle (1964). Expressions for these rates are set forth below, in which the units of R are $cm^{-3}sec^{-1}$, of ρ are gm/cm^3, of ρ_5 are $10^5 gm/cm^3$, of T_8 are 10^8 °K, and of T_9 are 10^9 °K.

The first three reactions, describing helium burning, are important in the temperature interval between $\log T = 7.9$ and $\log T = 8.4$; at the lower limit of this range the reactions occur in barely significant amounts, whereas at the upper limit they are so fast that no helium can long remain in the material without being consumed. The first of these reactions, the triple-alpha, involves a small equilibrium concentration of the unbound nucleus Be^8 in its ground state. This reacts with an alpha particle to yield the nucleus C^{12} in its 7.65 Mev excited state, which then decays by γ or $e^{\pm}$ emission to the C^{12} ground state. The reaction rate is given by

$$\log R_{12} = 16.45 + 3\log\left[\frac{\rho}{T_8}\right] - \frac{18.75}{T_8} + (0.38)\left[\frac{\rho_5}{T_8^3}\right]^{1/2} . \qquad (A64)$$

The second reaction involves the 7.116 Mev excited state of O^{16}, and has a rate given by (A65)

$$\log R_{16} = 33.54 + \log \theta_\alpha^2 + 2\log\left[\frac{\rho}{T_8}\right] - \frac{30.08}{T_8^{\frac{1}{3}}} - \frac{0.18}{T_8^{\frac{2}{3}}} + 0.38\left[\frac{\rho_5}{T_8^3}\right]^{1/2} .$$

Here the determination of θ_α^2 (the reduced alpha-particle width) is somewhat uncertain; $\theta_\alpha^2 = 0.78$ is used in these calculations. It is possible that a revised value of θ_α^2 could reduce $\log R_{16}$ by as much as unity from the values calculated in this work; this would have an important effect on the carbon-oxygen ratio in the product material.

The third reaction proceeds via three channels, an off-resonant one, one involving the 5.63 Mev excited state in Ne^{20}, and one involving the 5.80 Mev excited state in Ne^{20}. The rates used in this work for the three channels are given by

$$\log R_{20}^{a} = 33.27 + \log \theta_\alpha^2 + 2\log \rho - \frac{2}{3}\log T_8 - \frac{37.2}{T_8^{\frac{1}{3}}} + 0.51\left[\frac{\rho_5}{T_8^3}\right]^{1/2} \qquad \text{(A66)}$$

$$\log R_{20}^{b} = 25.37 + 2\log \rho - \frac{3}{2}\log T_8 - \frac{45.4}{T_8} + 0.51\left[\frac{\rho_5}{T_8^3}\right]^{1/2} \qquad \text{(A67)}$$

and

$$\log R_{20}^{c} = 26.37 + 2\log \rho - \frac{3}{2}\log T_8 - \frac{53.9}{T_8} + 0.51\left[\frac{\rho_5}{T_8^3}\right]^{1/2} . \qquad \text{(A68)}$$

According to Fowler (1964) more recent data require that the initial numbers in the above three equations be replaced by 32.77, 24.87, and 24.37 respectively. The total rate is the sum of the rates for the three channels:

$$R_{20} = R_{20}^{a} + R_{20}^{b} + R_{20}^{c} . \qquad \text{(A69)}$$

The older values appearing in equations A66 through A68, and the value $\theta_\alpha^2 = 1$, were used in this work; because this reaction did not occur significantly in the models, the numerical results would not be altered by small changes in these quantities.

The carbon and oxygen burning reactions listed in Table 12 are formal summaries of the major results of reactions among C^{12} and O^{16} nuclei; actually the reactions lead to the formation of several products, including neutrons and protons, the product nuclei having atomic wieghts distributed between 20 and 40. The rates are obtained simply from consideration of the lifetimes for compound nucleus formation among the reactants. They are given by

$$\log R_{24} = 49.30 + 2\log\rho - \frac{2}{3}\log T_9 - 36.57\left(\frac{1}{T_9} + 0.080\right)^{1/3} \qquad \text{(A70)}$$

$$\log R_{28} = 54.29 + 2\log\rho - \frac{2}{3}\log T_9 - 46.30\left(\frac{1}{T_9} + 0.080\right)^{1/3} \qquad \text{(A71)}$$

and

$$\log R_{32} = 60.27 + 2\log\rho - \frac{2}{3}\log T_9 - 59.04\left(\frac{1}{T_9} + 0.080\right)^{1/3} . \qquad \text{(A72)}$$

These reaction rates are non-negligible when $\log T > 8.7$ for material at densities of the order of 10^6 gm/cm^3.

Let Q_A represent the energy released in the reaction leading to the formation of the product nucleus with atomic weight A. The energy generated per unit time and per unit mass of stellar material is

$$\epsilon = \frac{Q_{12}}{\rho}(x_\alpha)^3 R_{12} + \frac{Q_{16}}{\rho}(x_\alpha)(x_{12})R_{16} + \frac{Q_{20}}{\rho}(x_\alpha)(x_{16})R_{20} + \frac{Q_{24}}{\rho}(x_{12})^2 R_{24} + \frac{Q_{28}}{\rho}(x_{12})(x_{16})R_{28} + \frac{Q_{32}}{\rho}(x_{16})^2 R_{32} . \qquad \text{(A73)}$$

The composition changes brought about by these reactions are examined in Section C-1.

APPENDIX B. DETERMINATION OF A STELLAR MODEL.

This appendix describes a method, based on the theory of stellar interiors, for the construction of a single numerical stellar model of total mass $\mathcal{M}$. The basic independent variable is taken as $\log M$ (for $M \leq (0.5)\mathcal{M}$) or $\log m$ (for $M > (0.5)\mathcal{M}$) and is specified at each of several mass levels, carrying the index J. The mass level nearest the surface is indicated by J = 1, that nearest the center by J = JAY, and the center itself by J = JC or simply by a subscript c. At each mass level the independent variables x_a through x_z specify the composition, and the dependent variables $\log r$, L/L_o (where L_o is a constant approximately equal to the luminosity of the star), $\log T$, and $\log P$ take on discrete numerical values; these values provide the substance of a stellar model. Numerical values for the auxiliary quantities ρ, κ, ϵ', and u and their logarithmic derivatives are also calculated at each mass level J. The following three sections describe the techniques used for the determination of satisfactory numerical values of the dependent variables.

Section B-1. The Trial Model.

In a satisfactory stellar model the dependent and auxiliary variables must be related in a way which satisfies the equations of stellar structure listed in Section I-3. To this end the equations are rewritten here as a set of quantities B1 through B15 each of which must be zero:

at the surface of the star:

$$f_g = \log\left[\frac{GmM}{4\pi r^4 P}\right] \tag{B1}$$

$$f_\sigma = \frac{8\pi r^2 \sigma T^4}{L} - 1 - \frac{3}{2}\int_0^m \kappa \frac{dm}{4\pi r^2} \tag{B2}$$

throughout the body of the star, for $M > (0.5)\mathcal{M}$:

$$g_r = -\frac{m}{r}\frac{dr}{dm} - \frac{m}{4\pi r^3 \rho} \tag{B3}$$

$$g_L = (2.303)\left[-\frac{m}{L_o}\frac{dL}{dm} - \frac{m}{L_o}\epsilon'\right] \tag{B4}$$

$$g_T = \begin{cases} -\dfrac{m}{T}\dfrac{dT}{dm} + \dfrac{3}{4ac}\dfrac{\kappa}{T^4}\dfrac{mL}{16\pi^2 r^4} \\ -\dfrac{m}{T}\dfrac{dT}{dm} + \dfrac{\Gamma_2 - 1}{\Gamma_2}\dfrac{GmM}{4\pi r^4 P} \end{cases} \tag{B5}$$

$$g_P = -\frac{m}{P}\frac{dP}{dm} + \frac{GmM}{4\pi r^4 P} \tag{B6}$$

throughout the body of the star, for $M \leq (0.5)\mathcal{M}$:

$$g_r = \frac{M}{r}\frac{dr}{dM} - \frac{M}{4\pi r^3 \rho} \tag{B7}$$

$$g_L = (2.303)\left[\frac{M}{L_o}\frac{dL}{dM} - \frac{M}{L_o}\epsilon'\right] \tag{B8}$$

$$g_T = \begin{cases} \dfrac{M}{T}\dfrac{dT}{dM} + \dfrac{3}{4ac}\dfrac{\kappa}{T^4}\dfrac{ML}{16\pi^2 r^4} \\ \dfrac{M}{T}\dfrac{dT}{dM} + \dfrac{\Gamma_2 - 1}{\Gamma_2}\dfrac{GM^2}{4\pi r^4 P} \end{cases} \tag{B9}$$

$$g_P = \frac{M}{P}\frac{dP}{dM} + \frac{GM^2}{4\pi r^4 P} \tag{B10}$$

and at the center of the star (here M is the mass interior to the mass level at J = JAY):

$$f_r = \log r - \frac{1}{3}\log\left[\frac{3M}{4\pi\rho_c}\right] \tag{B11}$$

$$f_L = \frac{L}{L_o} - \frac{M\epsilon'}{L_o} \tag{B12}$$

$$f_T = \frac{T + \tau - T_c}{T_c} \tag{B13}$$

where
$$\tau = \begin{cases} \dfrac{\kappa_c \epsilon'_c}{8acT_c^3}\rho_c^2\left[\dfrac{3M}{4\pi\rho_c}\right]^{2/3} \\ \dfrac{\Gamma_2 - 1}{\Gamma_2}\dfrac{2\pi G}{3}\dfrac{T_c}{P_c}\rho_c^2\left[\dfrac{3M}{4\pi\rho_c}\right]^{2/3} \end{cases} \tag{B14}$$

and, lastly, $$f_P = \frac{P + \varphi - P_c}{P_c} \tag{B15}$$

where $$\varphi = \frac{2\pi G}{3}\rho_c^2\left[\frac{3M}{4\pi\rho_c}\right]^{2/3} . \tag{B16}$$

The choice between the radiative and convective forms of g_T and f_T is, as usual, made to yield the less negative of the two possible values for the logarithmic temperature derivative

$$\frac{d\log T}{d\log M} = \frac{M}{T}\frac{dT}{dM} . \tag{B17}$$

From the independent and dependent variables of the trial model we proceed first to the evaluation of the auxiliary quantities and thence to the evaluation of the expressions f_g through f_p, as

follows. At the first mass level, subscripted 1, equation B1 yields

$$f_g = \log \frac{G}{4\pi} + \log \mathcal{M} + \log m_1 - 4 \log r_1 - \log P_1 \quad . \tag{B18}$$

The integral in f_σ (cf. equation B2) is evaluated by

$$\frac{3}{2} \int_0^{m_1} \frac{\kappa \, dm}{4\pi r_1^2} = \frac{3\kappa_1 m_1}{8\pi r_1^2} \int_0^1 y dx \tag{B19}$$

where $x = m/m_1$ and $y = \kappa/\kappa_1$; at each value of x we obtain the opacity κ using

$$\log T = \log T_e + \frac{1}{4} \log \left[\frac{1}{2} \left(1 + \frac{3}{2} \tau\right)\right] \tag{B20}$$

and

$$\log \rho = \log \rho_1 + \log \left[\frac{P - P_r}{P_1 - \frac{a}{3} T_1^4} \right] - \log \frac{T}{T_1} \tag{B21}$$

where

$$P_r = \frac{a}{3} T^4 \left[\frac{3\tau/2}{1 + 3\tau/2} \right] \tag{B22}$$

and

$$\frac{3}{2} \tau = \frac{3\kappa_1 m_1}{8\pi r_1^2} \int_0^x y dx \quad . \tag{B23}$$

In order to discuss g_r, g_L, g_T, and g_P we consider the representative equation

$$\frac{dy}{dx} = f(x) \quad . \tag{B24}$$

At the points x_1, x_2, and x_3 let the function f(x) have the values f_1, f_2, and f_3. Then we can approximate f(x) in the region between x_1 and x_2 by (B25)

$$f(x) \approx \frac{f_1 + f_2}{2} + \left[x - \frac{x_1 + x_2}{2} \right] \left[\frac{f_2 - f_1}{x_2 - x_1} \right] + (x - x_1)(x - x_2) \frac{f''}{2} \quad .$$

By requiring that $f(x)$ have the value f_3 at x_3 we can obtain

$$\frac{f''}{2} = \frac{(x_2 - x_1)f_3 + (x_3 - x_2)f_1 + (x_1 - x_3)f_3}{(x_2 - x_1)(x_3 - x_1)(x_3 - x_2)} \quad . \tag{B26}$$

Integrating equation B24 to find $(y_2 - y_1)$ yields

$$\begin{aligned}(y_2 - y_1) &= \int_{x_1}^{x_2} f(x)dx \\ &\approx (x_2 - x_1)\left[\left(\frac{f_1 + f_2}{2}\right) - \frac{(x_2 - x_1)^2}{6}\frac{f''}{2}\right]\end{aligned} \tag{B27}$$

Associating x_1 with $\log M_{J-1}$, x_2 with $\log M_J$, y_1 with $\log r_{J-1}$, and y_2 with $\log r_J$ and letting

$$f(x) = \frac{M}{4\pi r^3 \rho} \quad , \tag{B28}$$

we can evaluate g_r at the adjacent points (J-1) and J as follows:

$$(g_r)_J = \frac{\log r_{J-1} - \log r_J}{\log M_{J-1} - \log M_J} - \left[\left(\frac{f_{J-1} + f_J}{2}\right) - \frac{(\log M_J - \log M_{J-1})^2}{6}\frac{f''}{2}\right] \quad . \tag{B29}$$

Three points are required for the evaluation of $f''/2$ via equation B26; in practice it is taken as an average of $f''/2$ evaluated at (J-2), (J-1), and J and of $f''/2$ evaluated at (J-1), J, and (J+1). The quantities $(g_L)_J$, $(g_T)_J$, and $(g_P)_J$ may be obtained analogously, for both the internal and external forms.

The quantities f_r, f_L, f_T, and f_P, at the center of the star, may be directly calculated from equations B11 through B16.

The foregoing material permits the evaluation, for the trial model, of the 4(JAY)+2 expressions f_g through f_p of equations B1 through B15. If these are not all zero to within some desired accuracy the model is not satisfactory. The following section describes the iterative procedure used to obtain an improved model.

Section B-2. Iterations on the Trial Model.

The dependent variables of the trial model are $\log r$, L/L_o, $\log T$, and $\log P$; let the values of f_g through f_p for this model be given superscripts o. In an improved model the variables are to be replaced by

$$\begin{aligned} &\log r + [r] \\ &L/L_o + [L] \\ &\log T + [T] \\ &\log P + [P] \end{aligned} \tag{B30}$$

where the unknown quantities [r], [L], [T], and [P] are to be small compared to unity. Let A denote $\ln 10 = 2.303$. Then for the new model the expressions f_g through f_p will be given approximately as follows: at the surface

$$f_g = (f_g)^o - 4[r]_1 - [P]_1 \tag{B31}$$

$$\text{and } f_o = \left[\frac{8\pi r_1^2 \sigma T_1^4}{L_1}\right]^o \left(1 + 2A[r]_1 + 4A[T]_1 - \frac{L}{L_1}[L]_1\right) - 1$$

$$- \left[\frac{3}{2}\int_0^{m_1} \frac{\chi\, dm}{4\pi r_1^2}\right]^o \left(1 + A\left[\frac{T}{\chi}\frac{\partial \chi}{\partial T}\right]_1 [T]_1 + A\left[\frac{P}{\chi}\frac{\partial \chi}{\partial P}\right]_1 [P]_1 - 2A[r]_1\right) . \tag{B32}$$

Within the star

$$(g_r)_J = (g_r)^o_J + \frac{[r]_{J-1} - [r]_J}{\ell\log M_{J-1} - \ell\log M_J}$$

$$- \frac{1}{2}\left[\frac{M}{4\pi r^3 \rho}\right]^o_{J-1}\left(-3A[r]_{J-1} - A\left[\frac{T}{\rho}\frac{\partial\rho}{\partial T}\right]_{J-1}[T]_{J-1} - A\left[\frac{P}{\rho}\frac{\partial\rho}{\partial P}\right]_{J-1}[P]_{J-1}\right)$$

$$- \frac{1}{2}\left[\frac{M}{4\pi r^3 \rho}\right]^o_{J}\left(-3A[r]_{J} - A\left[\frac{T}{\rho}\frac{\partial\rho}{\partial T}\right]_{J}[T]_{J} - A\left[\frac{P}{\rho}\frac{\partial\rho}{\partial P}\right]_{J}[P]_{J}\right); \quad \text{(B33)}$$

similar expressions for $(g_L)_J$, $(g_T)_J$, and $(g_P)_J$ may be easily obtained. The term containing $f''/2$ has been included in $(g_r)^o_J$ but not in the remaining terms. Near the center we obtain

$$f_r = f^o_r + [r]_{JAY} + \frac{1}{3}\left[\frac{T}{\rho}\frac{\partial\rho}{\partial T}\right]_c[T]_c + \frac{1}{3}\left[\frac{P}{\rho}\frac{\partial\rho}{\partial P}\right]_c[P]_c \quad \text{(B34)}$$

and

$$f_L = f^o_L + [L]_{JAY} - \frac{M_{JAY}}{L_o}\epsilon'_c\left(A\left[\frac{T}{\epsilon'}\frac{\partial\epsilon'}{\partial T}\right]_o[T]_c + A\left[\frac{P}{\epsilon'}\frac{\partial\epsilon'}{\partial P}\right]_c[P]_c\right). \quad \text{(B35)}$$

Expressions for f_T and f_P may be obtained analogously.

Let the row vector $\underset{\sim}{x}$ have as its elements the $4(JAY)+2$ unknowns, in order,

$$\underset{\sim}{x} = \{\, [r]_1, [L]_1, [T]_1, [P]_1, [r]_2, [L]_2, \ldots .$$
$$\ldots . [T]_{JAY}, [P]_{JAY}, [T]_c, [P]_c \,\} \quad \text{(B36)}$$

and the column vector $\underset{\sim}{B}$ have as its elements the $4(JAY)+2$ quantities evaluated using the trial model,

$$\underset{\sim}{B} = \{\, f^o_g, f^o_\sigma, (g_r)^o_2, (g_L)^o_2, (g_T)^o_2, (g_P)^o_2, \ldots .$$
$$\ldots . (g_T)^o_{JAY}, (g_P)^o_{JAY}, f^o_r, f^o_L, f^o_T, f^o_P \,\} . \quad \text{(B37)}$$

The system of equations describing the setting of the 4(JAY)+2 quantities f_g through f_p equal to zero may be cast in the form

$$\underset{\sim}{B} - \underset{\sim}{A}\,\underset{\sim}{x} = 0 \quad . \tag{B38}$$

The matrix $\underset{\sim}{A}$ has all of its non-zero elements clustered near the diagonal, as diagrammed in Figure 15. The solution of the system B38 for the elements of $\underset{\sim}{x}$ takes advantage of the special form of $\underset{\sim}{A}$, and is accomplished by the following procedure.

The first two equations can be solved for $[r]_1$ and $[L]_1$ as linear combinations of $[T]_1$ and $[P]_1$. These may be substituted in the third through sixth equations, which then form a system of four equations in six unknowns. A standard technique for the inversion of a four-by-four matrix is then used to solve for four of these unknowns, $[T]_1$, $[P]_1$, $[r]_2$, and $[L]_2$, in terms of the remaining two, $[T]_2$ and $[P]_2$. The substitution of two of these four linear forms in the next four equations permits solution for four more unknowns in terms of $[T]_3$ and $[P]_3$. Repeated application of the substitutions and solutions leads to the situation in which $[r]_{JAY}$ and $[L]_{JAY}$ are expressed in terms of $[T]_{JAY}$ and $[P]_{JAY}$. The substitution of these two linear forms into the last four equations leaves four equations in the four unknowns $[T]_{JAY}$, $[P]_{JAY}$, $[T]_c$, and $[P]_c$. One more application of the matrix-inversion scheme provides numerical values for these four unknowns. Then by successive substitution values for all 4(JAY)+2 unknown elements of the vector $\underset{\sim}{x}$ can be obtained.

As the numerical value of each unknown is obtained its size is examined. The linearization exhibited in equations B31 and B35 (and in the several others like them) is meaningful only if the changes in all the physical quantities are small. This may be assured by requiring the absolute values of $[r]_J$, $(0.434)[L]_J$, $t[T]_J$, and $p[P]_J$ (for all levels J) to be less than some number, taken in these calculations as 0.13, corresponding to a maximum fractional change of 35 per cent in any physical quantity. Here t is the largest in absolute value among $\left[\frac{T}{\rho}\frac{\partial\rho}{\partial T}\right]_J$, $\left[\frac{T}{\kappa}\frac{\partial\kappa}{\partial T}\right]_J$, $\left[\frac{T}{\epsilon''}\frac{\partial\epsilon'}{\partial T}\right]_J$, and unity and p is the largest in absolute value among $\left[\frac{P}{\rho}\frac{\partial\rho}{\partial P}\right]_J$, $\left[\frac{P}{\kappa}\frac{\partial\kappa}{\partial P}\right]_J$, $\left[\frac{P}{\epsilon''}\frac{\partial\epsilon'}{\partial P}\right]_J$, and unity, where ϵ'' is the largest of the $|\epsilon''|$ encountered in the star. If an element of $\underset{\sim}{x}$ exceeds this requirement it is replaced by a number with the same sign and an absolute value satisfying the requirement, before proceeding further in the sequence of substitutions by which the remaining elements of $\underset{\sim}{x}$ are to be calculated.

If at each mass level J the quantities $\log r$, L/L_o, $\log T$, and $\log P$ of the trial model are replaced by those of form B30 a new trial model is obtained. In order to satisfy the requirement that $\log r$, $\log T$, and $\log P$ be monotonic from center to surface we check the new model for inversions in these quantities; if such are found we simply redistribute the dependent variables among the mass levels, eliminating the inversions. For the trial model the expressions B1 through B16 may be evaluated; each such iteration should bring these expressions closer to zero. A trial model becomes an acceptable stellar

model if all the inequalities B40 through B42 are satisfied. For each value of J let

$$G = \begin{cases} (2.303)(\log m_J - \log m_{J-1}) & \text{for } M \geq (0.5)\mathcal{M} \\ (2.303)(\log M_{J-1} - \log M_J) & \text{for } M < (0.5)\mathcal{M}. \end{cases} \tag{B39}$$

The surface equations demand

$$(2.303)|f_g| \quad \text{and} \quad \left|\frac{L_o f_\sigma}{8\pi r^2 \sigma T^4}\right| < q \quad . \tag{B40}$$

At each mass level J, letting $(g_r)_J$ and similar forms be specified by equations like B29, demand

$$|G(g_r)_J|, \ \left|\frac{G}{2.303}(g_L)_J\right|, \ |G(g_T)_J|, \text{ and } |G(g_P)_J| < q \quad . \tag{B41}$$

At the center demand

$$(2.303)|f_r|, \ |f_L|, \ |f_T|, \text{ and } |f_p| < q \quad . \tag{B42}$$

In these calculations the maximum permissible fractional error q was taken to be 10^{-4}. For the evolutionary models about four iterations were usually sufficient to proceed from a trial model predicted from models at previous times to an acceptable current model, requiring about forty seconds of computing time.

Section B-3. The Mass Level Structure.

The distribution of those discrete values of M which were to be assigned to the mass levels J was determined by the following considerations. The error (which results from the lack of an infinitely fine sequence of mass levels) is displayed by the term proportional

to $f''/2$ in equation B29. For a pair of nearby mass levels J and J' the machine computes the $f''/2$ terms for each of the four stellar interior equations, chooses the largest in absolute value from among the four, and examines

$$\frac{1}{6}\left(\log M_J - \log M_{J'}\right)^3 \frac{f''}{2} \quad . \tag{B43}$$

It requires this quantity to be smaller than $n^3 q$ where the integer n is $|J - J'|$ and q is some small number. The machine inserts or deletes mass levels in the interval (J,J') to keep in step with this criterion, such that the terms proportional to $f''/2$ never contribute more than q to the logarithms of the dependent variables. These terms are nevertheless included in the model calculations. A $q = 10^{-3}$ led to the use of about 100 mass levels, which were adjusted every few evolutionary time steps.

APPENDIX C. THE EVOLUTIONARY CALCULATIONS.

This appendix discusses the creation of sequential models describing the evolution of a star. A pair of such models must satisfy the requirements

(a) that the composition change between them satisfy in detail the appropriate set of differential equations C5 through C8;

(b) that the energy release at each point in the star resulting from gravitational contraction be included in the energy generation equations 1.11 and C13; and

(c) that the difference in the total energy stores of the two model stars, summing the nuclear, thermal, and gravitational energy contents, equal the total energy radiated in the time interval between the two models.

The physics employed in the construction of the models guarantees that condition (c) is satisfied automatically when (a) and (b) are satisfied by the detailed structures of the models. The following two sections detail the numerical procedures used in the construction of models satisfying requirements (a) and (b). The third section describes procedures used to obtain a trial model in the evolutionary sequence, and to choose appropriate time steps between models.

Section C-1. Change in Chemical Composition.

Nuclear reactions are accompanied by composition changes which play an important role in stellar evolution. The consideration of the reactions listed in Table 12 and described in Section A-3 leads to the following equations for the transformation rates:

$$\frac{dn_\alpha}{dt} = \frac{\rho}{4H}\frac{dx_\alpha}{dt} \qquad (C1)$$
$$= -3(x_\alpha)^3 R_{12} - (x_\alpha)(x_{12})R_{16} - (x_\alpha)(x_{16})R_{20}$$

$$\frac{dn_{12}}{dt} = \frac{\rho}{12H}\frac{dx_{12}}{dt} \qquad (C2)$$
$$= +(x_\alpha)^3 R_{12} - (x_\alpha)(x_{12})R_{16} - 2(x_{12})^2 R_{24} - (x_{12})(x_{16})R_{28}$$

$$\frac{dn_{16}}{dt} = \frac{\rho}{16H}\frac{dx_{16}}{dt} \qquad (C3)$$
$$= +(x_\alpha)(x_{12})R_{16} - (x_\alpha)(x_{16})R_{20} - (x_{12})(x_{16})R_{28} - 2(x_{16})^2 R_{32}$$

and $$\frac{dn_{20}}{dt} = \frac{\rho}{20H}\frac{dx_{20}}{dt} \qquad (C4)$$
$$= +(x_\alpha)(x_{16})R_{20} \quad .$$

These equations would be valid at each instant at every point in the star were it not for the fact that in a convective region the fractions by mass and their rates of change must be uniform throughout. In order to cast the equations for the static mass points and for the convective regions in the same form we set

$$\frac{dx_\alpha}{dt} = 4\left[-3(x_\alpha)^3 R'_{12} - (x_\alpha)(x_{12})R'_{16} - (x_\alpha)(x_{16})R'_{20}\right] \qquad (C5)$$

$$\frac{dx_{12}}{dt} = 12\left[+(x_\alpha)^3 R'_{12} - (x_\alpha)(x_{12})R'_{16} - 2(x_{12})^2 R'_{24} - (x_{12})(x_{16})R'_{28}\right] \tag{C6}$$

$$\frac{dx_{16}}{dt} = 16\left[(x_\alpha)(x_{16})R'_{16} - (x_\alpha)(x_{16})R'_{20} - (x_{12})(x_{16})R'_{28} - 2(x_{16})^2 R'_{32}\right] \tag{C7}$$

and $$\frac{dx_{20}}{dt} = 20\left[(x_\alpha)(x_{16})R'_{20}\right] \quad . \tag{C8}$$

Values for x_z, the fraction by mass of elements having atomic weights greater than 20, are provided by the relation

$$x_\alpha + x_{12} + x_{16} + x_{20} + x_z = 1 \quad . \tag{C9}$$

For a mass level in a non-convective region we simply set each

$$R' = \frac{H}{\rho} R \quad . \tag{C10}$$

For a region convective in the interval (M_1, M_2) we set each

$$R' = \frac{H}{M_2 - M_1} \int_{M_1}^{M_2} R \frac{dM}{\rho} \quad . \tag{C11}$$

We have now to deal with the time development of the solutions of equations C5 through C8 for the composition parameters at each level, choosing values of R' appropriate for either stable or convective regions.

Consider two successive models for each of which values of $\log T$, $\log \rho$, and ψ (convection parameter; cf. equation 1.5) are specified at the mass levels M_J, and for the first of which the composition parameters are also specified in detail. These correspond respectively to an accepted model at a former evolutionary

time and to the trial model at the current time. For those pairs of adjacent mass levels J and J' in each model between which the convection indicator ψ changes sign we assume M_1, the mass interior to the convective zone boundary, to be given by

$$\log M_1 = (\psi_J \log M_{J'} - \psi_{J'} \log M_J)/(\psi_J - \psi_{J'}) \qquad (C12)$$

Between the two models we assume that the quantities $\log M_1$ at all convective zone boundaries and $\log T$ and $\log \rho$ at all mass levels are linear with time. On the basis of these assumptions we can compute a value for each R' at all intermediate times for each stable mass layer and for each convective region. Sufficient information is now available so that a Runge-Kutta integration of the composition changing equations C5 through C8 can be performed to derive values for the composition parameters appropriate for the trial model at the current time. In this Runge-Kutta integration the time steps can be chosen much smaller than the time step between the models, in order to insure reliable computation of the new composition.

Section C-2. Gravitational Contraction.

The contribution of the gravitational contraction to the energy generation, described by equation 1.11, is obtained as follows. Let subscripts a refer to the accepted model at the former evolutionary time t_a and subscripts b to the trial model at the current time t_b. Then for computational purposes we replace equation 1.11 at each

mass level by

$$\epsilon'_b = \epsilon_b - \frac{u_b - u_a}{t_b - t_a} - \frac{P_a + P_b}{2}\frac{\left[\frac{1}{\rho_b} - \frac{1}{\rho_a}\right]}{(t_b - t_a)} \quad . \qquad (C13)$$

Here ϵ_b is the nuclear energy generation rate obtained from the values of $\log T$, $\log \rho$, and the composition of the trial model at the time t_b, via equation A73.

Section C-3. Time Step and Model Prediction.

Given acceptable models at times t_a and t_b the continuation of the evolutionary sequence demands that a trial model be obtained at some new time t_c. It was found that this time could be suitably chosen using the formula

$$\log\left[\frac{t_c - t_b}{t_b - t_a}\right] = 0.8(q - 0.9) \quad . \qquad (C14)$$

Here q is the change per iteration in the logarithm of the greatest error (cf. forms B40 through B42) in the model at time t_b. The restriction that the time step $(t_c - t_b)$ not exceed twice the time step $(t_b - t_a)$ was also imposed. In this way convergence reducing the error by nearly a factor of ten per iteration is maintained throughout the evolutionary calculations. Such a scheme for the choice of the time step seems to be most efficient, in that it permits the evolution to proceed as far as possible in a given amount of computer time.

A linear extrapolation in time was used to set up the trial model at the new time t_c. Let y represent any of the quantities $\log r$, L/L_o, $\log T$, $\log P$, $\log \rho$, and ψ at each of the mass levels; the extrapolation formula

$$y_c = y_b + \frac{t_c - t_b}{t_b - t_a}(y_b - y_a) \qquad (C15)$$

is used to predict the new model values. From the trial model so obtained the new composition is predicted on the basis of the material in Section C-1. For this composition new auxiliary quantities are computed and the model is tested according to the requirements of Section B-1. If the model is not satisfactory it is altered as described in Section B-2. Iterations are performed in this way until an acceptable model is obtained, and then preparations are made for a subsequent time step. Thus a series of models describing the evolution of a helium star can be obtained and printed out.

Each time a few evolutionary models are created the current and former models are stored on magnetic tape, so that they may be accessible at a later time when the evolutionary computations are to be continued.

APPENDIX D. NOTATION.

This appendix tabulates the symbols which represent various physical and numerical quantities. It presents for each symbol a description, the units in which it was used throughout the computations, and the section in which it is introduced in this report. The meanings of the several subscripts are also included. First are presented intrinsic quantities related to the description of stellar material. The second section presents extrinsic quantities which are used to describe a star and extrinsic quantities related to a thermodynamic system (cf. Section A-1). The third and last section lists the constants used, for all of which the numerical values tabulated by Allen (1963) have been adopted. Many symbols of limited usage are omitted, as are conventional mathematical symbols.

Section D-1. Intrinsic Quantities.

symbol	subscripts	description	units	introduced by Section
A		atomic weight	(none)	A-1
E		electron energy	ergs	A-1
F_s		Fermi-Dirac functions	(none)	A-1
I^s		degeneracy integral	(none)	A-1
	N	number		
	P	pressure		
	U	energy		
n		composition fraction by number	(none)	C-1
	$\alpha, 12 \ldots$	He^4, C^{12}, etc.		
p		electron momentum	gm-cm/sec	A-1
P		pressure	$ergs/cm^3$	I-3
	a	ion		
	c	central		
	e	electron		
	r	radiation		
Q_A		energy release per reaction leading to creation of nucleus with atomic weight A	ergs, Mev	A-3
R_A		reaction rate leading to creation of nucleus with atomic weight A	$\frac{\text{reactions}}{cm^3 \text{ sec}}$	A-3
t		time	sec, years	I-3
T		temperature	$^\circ K$	I-3
	c	central		
	e	effective		
u		internal energy density	ergs/gm	I-3
u		electron energy parameter	(none)	A-1

symbol	subscripts	description	units	introduced by Section
U_r		partition function	(none)	A-1
U_z		energy of ionization	ergs, ev	A-1
x		composition fraction by mass	(none)	II
	α,12....	He^4, C^{12}, etc.		
	Z	element of atomic number Z		
Z		atomic number	(none)	A-1
Z'		average number of free electrons per atom	(none)	A-1
α,ν		degeneracy parameters	(none)	A-1
β		gas pressure fraction	(none)	II-2
γ		ratio of specific heats	(none)	A-1
Γ_2		adiabatic exponent	(none)	I-3
ε		electron temperature parameter	(none)	A-1
ε,ε′		energy generation rates	ergs/gm sec	I-3
κ		Rosseland mean opacity	cm^2/gm	I-3
	R	radiative		
Λ		degeneracy indicator	(none)	A-1
μ		molecular weight	amu/particle	A-1
	a	ion		
	e	electron		
ν_c		electron conductivity	erg/cm sec ^oK	A-1
ρ		density	gm/cm^2	I-3
	c	central		
χ_r		ionization potential	ergs, ev	A-1
ψ		convection parameter	(none)	I-3

Section D-2. Extrinsic Quantities.

symbol	subscripts	description	units	introduced by Section
For a star model:				
L		internal luminosity variable	ergs/sec	I-3
	o	arbitrary constant		
$\mathcal{L}$		external luminosity	ergs/sec	II-3
m		exterior mass variable	gm	I-3
M		interior mass variable	gm	I-3
	f	at core edge		
$\mathcal{M}$		total mass	gm	I-3
M		absolute magnitude	(none)	II-1
	bol	bolometric		
	pg	photographic		
r		internal radius variable	cm	I-3
	f	at core edge		
R		exterior radius	cm	II-1
τ		optical depth	(none)	I-3
For a thermodynamic system:				
M		mass	gm	A-1
N		number of particles	(none)	A-1
	a	ions		
	e	electrons		
	r	atoms r times ionized		
	z	of atomic number Z		
U		energy content	ergs	A-1
	a	ions (thermal kinetic)		
	e	electrons (thermal kinetic)		
	i	of ionization		
	r	radiation		
V		volume	cm^3	A-1

Section D-3. Constants.

description	symbol	value
Laboratory constants:		
radiation density constant	a	$7.5641\ 10^{-15}$ erg/cm^3 $^\circ$K^4
speed of light	c	$2.997929\ 10^{10}$ cm/sec
gravitational constant	G	$6.668\ 10^{-8}$ erg-cm/gm^2
Planck's constant	h	$6.6252\ 10^{-27}$ erg sec
mass of hydrogen atom	H	$1.67333\ 10^{-24}$ gm
Boltzmann's constant	k	$1.38046\ 10^{-16}$ erg/$^\circ$K
mass of the electron	m	$9.1084\ 10^{-28}$ gm
Stefan-Boltzmann constant	σ	$5.6692\ 10^{-5}$ erg/cm^2 sec $^\circ$K^4
energy conversion factor		$1.60207\ 10^{-12}$ erg/ev
Astronomical constants:		
luminosity of the sun	$\mathcal{L}_\odot$	$3.90\ 10^{33}$ erg/sec
mass of the sun	$M_\odot$	$1.989\ 10^{33}$ gm
absolute bolometric magnitude of the sun	$(M_{bol})_\odot$	+4.72
radius of the sun	$R_\odot$	$6.9598\ 10^{10}$ cm
time conversion factor		$3.155693\ 10^7$ sec/year

REFERENCES.

Allen, C.W.	1963	Astrophysical Quantities (Second Edition; London: Athlone Press)
Aller, L.H.	1959	"Nuclei of Planetary Nebulae and the Late Stages of Stellar Evolution" Modèles d'Etoiles et Evolution Stellaire, 41 (Liège: Cointe-Sclessin)
Arp, H.C.	1958	"The Hertzsprung-Russell Diagram" Handbuch der Physik 51, 75
Arp, H.C.	1962	"The Globular Cluster M5" Ap. J. 135, 311
Castor, J.I.	1962	Private communication
Chandrasekhar, S.	1939	An Introduction to the Study of Stellar Structure (Chicago: University of Chicago Press; reprinted 1957 by Dover Publications, Inc.)
Cox, A.N.	1963	"Stellar Absorption Coefficients and Opacities" (unpublished; Los Alamos, New Mexico)
Cox, A.N.	1964	Preliminary Opacity Tabulation (unpublished; Los Alamos, New Mexico)
Cox, J.P., and Giuli, R.T.	1961	"Equilibrium Models for Stars which Derive Energy from Helium Burning. I. Stars Composed of Pure Helium." Ap. J. 133, 755
Cox, J.P., and Salpeter, E.E.	1961	"....II. Helium Stars with Hydrogen-Rich Envelopes." Ap. J. 133, 764
Cox, J.P., and Salpeter, E.E.	1964	"....III. Semi-Degenerate Stars of Small Mass." Ap. J. 140, 485
Deinzer, W., and Salpeter, E.E.	1964	"....IV. Massive Stars and Nuclear Abundances." Ap. J. 140, 499

Crawford, J.A.	1953	"Stars with Helium Energy Sources" Publ. Astron. Soc. Pacific 65, 210
Fowler, W.A., and Hoyle, F.	1964	Neutrino Processes and Pair Formation in Massive Stars and Supernovae (Ap.J. Supplements No. 91, Vol. IX)
Fowler, W.A.	1964	Private communication
Greenstein, J.L.	1960	"Spectra of Stars below the Main Sequence" Stellar Atmospheres, 676 (J.L. Greenstein, Ed.; Chicago: University of Chicago Press)
Greenstein, J.L.	1965	"Subluminous Stars" Galactic Structure, p. -- (Blaauw and Schmidt, Editors; Chicago: University of Chicago Press)
Harman, R.J., and Seaton, M.J.	1964	"The Central Stars of Planetary Nebulae" Ap. J. 140, 824
Hayashi, C., Hoshi, R., and Sugimoto, D.	1963	"Evolution of the Stars" Suppl. Progr. Theor. Physics, No. 22
Henyey, L.G., Forbes, J.E., and Gould, N.L.	1964	"A New Method of Automatic Computation of Stellar Evolution" Ap. J. 139, 306
Kuhi, L.V.	1964	Private communication
Kumar, Shiv S.	1963	"The Structure of Stars of Very Low Mass" Ap. J. 137, 1121
Kushwaha, R.S.	1957	"The Evolution of Early Main Sequence Stars" Ap. J. 125, 242
Limber, D. Nelson	1964	"The Wolf-Rayet Phenomenon" Ap. J. 139, 1251
McDougall, J., and Stoner, E.S.	1938	"The Computation of Fermi-Dirac Functions" Phil. Trans. Roy. Soc. London A 237, 67

Mestel, L.	1950	"On the Thermal Conductivity in Dense Stars" Proc. Camb. Phil. Soc. 46, 331
O'Dell, C.R.	1963	"The Evolution of Central Stars of Planetary Nebulae" Ap. J. 138, 67
Oke, J.B.	1961	"Model for a Helium Star of 1 Solar Mass" Ap. J. 133, 166
Osaki, Y.	1963	"Evolution of Helium Burning Stars of 0.8 Solar Masses" Publ. Astron. Soc. Japan 15, 428
Rublev, S.V.	1963	"Spectrophotometric Temperatures, Absolute Magnitudes, and Intrinsic Colors of Wolf-Rayet Stars" Soviet Astronomy AJ 7, 75
Sandage, Allan	1962	"The Ages of M67, NGC 188, M3, M5, and M13 According to Hoyle's 1959 Models" Ap. J. 135, 349
Schwarzschild, M.	1958	Structure and Evolution of the Stars (Princeton: Princeton University Press)
Traving, G.	1962	"The Atmospheres of Two B-Type Stars in the Galactic Halo" Ap. J. 135, 439
Van der Borght, R., and Meggitt, S.	1963	"Equilibrium Models of Pure Helium Stars" Australian J. of Physics 16, 68
Underhill, Anne B.	1960	"Early-Type Stars with Extended Atmospheres" Stellar Atmospheres, 411 (J.L. Greenstein, Ed.; Chicago: University of Chicago Press)

	small mass	intermediate mass		large mass
$\mathcal{M}/M_\odot$	0.33	1.0	10	200
$R/R_\odot$	0.05	0.2	0.8	4
$\mathcal{L}/\mathcal{L}_\odot$	4	300	10^5	10^7
M_{bol}	3	-2	-8	-12
$\log T_e$	4.6	4.8	5.0	5.2
$\log T_c$	8.02	8.12	8.27	8.37
$\log \rho_c$	5	4	3	2
q_f	0.3	0.3	0.7	0.97
$\frac{\partial \log L}{\partial \log M}$	7	3	2	1.2

Table 1. Order of magnitude of various quantities for homogeneous helium stars. The notation of the first seven rows is explained in Appendix D; q_f represents the mass fraction in the convective core, and $\frac{\partial \log L}{\partial \log M}$ is the slope of the mass-luminosity relation.

r/R	M/$\mathfrak{M}$	L/$\mathfrak{L}$	log T	log P	log ρ	κ
1.0000	1.00000	1.0000	4.9731	6.3611	-6.4419	4.488
0.9988	1.00000	1.0000	5.1482	7.0687	-5.9089	4.743
0.9969	1.00000	1.0000	5.3248	7.7778	-5.3762	4.507
0.9942	1.00000	1.0000	5.4830	8.4883	-4.8176	3.247
0.9871	1.00000	1.0000	5.7107	9.6984	-3.8192	1.487
0.9771	1.00000	1.0000	5.9386	10.7717	-2.9689	1.072
0.9639	1.00000	1.0000	6.1368	11.6733	-2.2632	0.975
0.9433	1.00000	1.0000	6.3388	12.5861	-1.5506	0.775
0.9051	0.99996	1.0000	6.5847	13.6582	-0.7233	0.573
0.8563	0.99969	1.0000	6.7769	14.5825	0.0103	0.422
0.7856	0.99789	1.0000	6.9993	15.5363	0.7419	0.358
0.6922	0.98794	1.0000	7.2218	16.4710	1.4536	0.350
0.5793	0.94500	1.0000	7.4365	17.3709	2.1374	0.320
0.4164	0.73905	1.0000	7.7051	18.4362	2.9297	0.247
0.3207	0.50000	1.0000	7.8482	18.9520	3.2992	0.240
0.2669	0.34581	1.0000	7.9258	19.1887	3.4568	0.222
0.2387	0.26844	1.0000	7.9646	19.2950	3.5237	0.210
0.2370	0.26394	1.0000	7.9668	19.3010	3.5274	
0.2353	0.25963	1.0000	7.9691	19.3068	3.5310	-0.209
0.1665	0.10816	0.9963	8.0464	19.5094	3.6550	-0.190
0.1104	0.03457	0.8681	8.0889	19.6219	3.7241	-0.182
0.0735	0.01065	0.5136	8.1073	19.6707	3.7541	-0.178
0.0394	0.00168	0.1249	8.1177	19.6984	3.7712	-0.176
0.0199	0.00022	0.0186	8.1209	19.7067	3.7763	-0.175
0.0068	0.00001	0.0008	8.1218	19.7092	3.7779	-0.175
0.0000	0.00000	0.0000	8.1219	19.7095	3.7781	-0.175

Table 2. Values of interior quantities for the homogeneous helium star model at one solar mass. The region of the convective core is indicated by prefixing a minus sign to the value of the opacity, and the core boundary is indicated by a single row.

$M/M_\odot$	$R/R_\odot$	$\mathcal{L}/\mathcal{L}_\odot$	M_{bol}	$\log T_e$	$\log T_c$	$\log P_c$	$\log \rho_c$	q_f	x_f
0.400	0.0774	5.446	+2.880	4.5028	8.0416	20.3887	4.4847	0.2183	0.2257
0.500	0.1001	15.786	+1.724	4.5627	8.0640	20.1815	4.2822	0.2238	0.2222
0.620	0.1235	38.664	+0.752	4.6142	8.0831	20.0155	4.1112	0.2304	0.2232
0.765	0.1491	86.951	-0.128	4.6613	8.1006	19.8724	3.9582	0.2443	0.2285
0.800	0.1550	102.728	-0.309	4.6711	8.1042	19.8439	3.9271	0.2475	0.2298
1.000	0.1866	230.00	-1.184	4.7182	8.1219	19.7096	3.7781	0.2640	0.2370
1.250	0.2228	496.93	-2.021	4.7634	8.1390	19.5875	3.6388	0.2825	0.2452
1.500	0.2563	908.3	-2.676	4.7984	8.1526	19.4957	3.5313	0.2971	0.2517
2.000	0.3166	2255	-3.663	4.8513	8.1732	19.3652	3.3727	0.3216	0.2630
3.000	0.4177	7409	-4.955	4.9203	8.2005	19.2108	3.1717	0.3720	0.2859
4.000	0.5023	16,157	-5.801	4.9649	8.2187	19.1229	3.0444	0.4307	0.3106
6.000	0.6447	44,380	-6.898	5.0204	8.2416	19.0351	2.8957	0.5289	0.3496
8.000	0.7635	84,662	-7.599	5.0538	8.2562	18.9910	2.8044	0.5962	0.3771
10.00	0.8700	134,714	-8.104	5.0759	8.2667	18.9656	2.7402	0.6417	0.3957
12.50	0.9885	207,623	-8.573	5.0951	8.2766	18.9460	2.6805	0.6873	0.4156
14.80	1.0896	283,337	-8.911	5.1077	8.2836	18.9349	2.6831	0.7224	0.4311
20.00	1.2969	476,842	-9.476	5.1264	8.2954	18.9214	2.5675	0.7768	0.4560
32.10	1.7183	1.01×10^6	-10.288	5.1465	8.3122	18.9135	2.4672	0.8435	0.4874
40.00	1.9695	1.39×10^6	-10.639	5.1521	8.3194	18.9142	2.4242	0.8657	0.4969
60.00	2.5500	2.44×10^6	-11.249	5.1569	8.3318	18.9207	2.3499	0.9011	0.5122

Table 3. Values of physical quantities for models at various masses on the helium star main sequence. Each row represents a particular model. The last two columns present respectively the mass and radius fractions at the edge of the convective core.

letter	surface event	letter	interior event
A	initial homogeneous model initial minimum	a	initial minimum T_c initial ρ_c
B, B'	minima of T_e	b	minimum ρ_c
C	maximum R	c	maximum T_c
D	minimum R	d	shell source appears
E, E'	maxima of T_e	e	$(He)_c$ falls below 0.008
F	maximum $\mathcal{L}$	f	convection ceases at center
G	minimum $\mathcal{L}$	g	minimum T_c
H	onset of convection near surface	h	shell source moves away from former core boundary
I	termination of model computation sequence		

Table 4. Letters assigned to various events in the evolutionary development of a helium star. In this and following tables the notation $(He)_c$ is equivalent to $(x_\alpha)_c$, the fraction by mass of He^4 at the center of the star.

model number	time in 10^6 years	events	increasing quantities	decreasing quantities	remarks
0	0.000	A, a			
			L, R, T_c, ρ_c	T_e, $(He)_c$	Mass in convective core and T_e are approximately constant
2 (2)	2.700 (2.129)	B			
			L, R, T_e, T_c, ρ_c	$(He)_c$	
8 (9)	9.400 (7.205)	C			
			L, T_e, T_c, ρ_c	R, $(He)_c$	mass in conv. core and L are approx. constant
21	12.170 (10.400)	D, c, d			
			L, R, T_e, ρ_c	T_c, $(He)_c$	
22	12.182 (10.550)	E, e			
			L, R, ρ_c	T_e, T_c	
24	12.242	f			
			L, R, ρ_c	T_e, T_c	T_e is approx. constant
31	12.509	B'			
			L, R, T_e, ρ_c	T_c	
34	13.100	g, h			
			L, R, T_e, T_c, ρ_c		core contracts, and shell source remains at approx. constant radius
43	15.385	E'			
			L, R, T_c, ρ_c	T_e	
69	16.704	H, I			

Table 5. (Caption on page 88).

model number	time in 10^6 years	$R/R_\odot$	M_{bol}	$\log T_e$	$M_f/M_\odot$	$r_f/R_\odot$	$\log T_c$	$\log \rho_c$
0	0.000	0.1867	-1.184	4.7182	0.264	0.0442	8.1219	3.7781
2	2.700	0.1969	-1.288	4.7170	0.267	0.0446	8.1308	3.7798
4	5.700	0.2076	-1.409	4.7175	0.267	0.0443	8.1455	3.7970
8	9.400	0.2146	-1.555	4.7249	0.267	0.0424	8.1794	3.8716
11	10.600	0.2116	-1.611	4.7336	0.267	0.0406	8.2019	3.9313
13	11.400	0.2032	-1.656	4.7470	0.267	0.0383	8.2303	4.0133
16	11.920	0.1890	-1.704	4.7675	0.267	0.0351	8.2679	4.1287
21	12.170	0.1786	-1.758	4.7852	0.267	0.0322	8.2957	4.2509
22	12.182	0.1788	-1.761	4.7853	0.267	0.0320	8.2946	4.2642
24	12.242	0.1880	-1.828	4.7810	0.267	0.0313	8.2672	4.3534
26	12.302	0.1989	-1.946	4.7805	0.267	0.0308	8.2408	4.4333
28	12.362	0.2071	-2.032	4.7803	0.268	0.0303	8.2241	4.4891
31	12.509	0.2183	-2.142	4.7800	0.268	0.0296	8.2016	4.5719
34	13.100	0.2321	-2.318	4.7842	0.314	0.0316	8.1847	4.7075
39	14.361	0.2540	-2.647	4.7976	0.388	0.0330	8.2193	4.8822
43	15.385	0.3032	-3.090	4.8034	0.464	0.0338	8.2725	5.0984
48	15.933	0.3844	-3.509	4.7939	0.523	0.0347	8.3273	5.2980
54	16.313	0.5667	-4.001	4.7587	0.584	0.0329	8.4031	5.5228
61	16.548	0.9785	-4.473	4.6873	0.643	0.0315	8.4825	5.7314
69	16.704	2.1967	-4.912	4.5556	0.701	0.0297	8.5597	5.9211

Table 6. (Caption on page 88).

Table 5.

Summary of the evolution of a helium star at one solar mass. In the first three columns are listed model numbers, evolutionary times, and events in the life of the star as obtained from the present investigation; entries in parentheses refer to the models which use a reduced rate for the reaction $C^{12}(\alpha,\gamma)O^{16}$ (cf. Section III-3). The last three columns indicate various developments which occur between the models specified at the left.

Table 6.

The evolution of a helium star at one solar mass. Values of various quantities are presented for selected models of the evolutionary sequence; each row represents one model. The sixth and seventh columns present in solar units respectively the mass and radius of a point having a helium content halfway between the central and surface values; early in the evolution this corresponds to the edge of the convective core, whereas later in the evolution it corresponds to the center of the shell source.

model number	time in 10^6 years	events	increasing quantities	decreasing quantities	remarks
0	0.00	A, a	L, R, T_c	T_e, ρ_c, $(He)_c$	mass in convective core and T_e are approximately constant
2	16.84	B, b	L, R, T_e, T_c, ρ_c	$(He)_c$	
8	59.66	C	L, T_e, T_c, ρ_c	R, $(He)_c$	mass in conv. core and L are approx. constant
19	79.12	D, c, d	L, R, T_e, ρ_c	T_c, $(He)_c$	
20	79.44	E, F, e	R, ρ_c	L, T_e, T_c	
23	79.60	G	L, R, ρ_c	T_e, T_c	
25	79.68	B', f	L, R, T_e, ρ_c	T_c	
37	84.11	g, h	L, T_e, T_c, ρ_c		core contracts, and R is approx. constant
54	131.39	I			

Table 7. Summary of the evolution of a helium star at 0.5 $M_\odot$; cf. Table 5.

model number	time in 10^6 years	$R/R_\odot$	M_{bol}	$\log T_e$	$M_f/M_\odot$	$r_f/R_\odot$	$\log T_c$	$\log \rho_c$
0	0.00	0.1001	+1.724	4.5627	0.112	0.0222	8.0640	4.2821
2	16.84	0.1052	+1.624	4.5618	0.114	0.0226	8.0699	4.2757
4	37.09	0.1102	+1.504	4.5637	0.114	0.0226	8.0831	4.2891
8	59.66	0.1132	+1.365	4.5719	0.114	0.0218	8.1106	4.3465
12	69.56	0.1104	+1.304	4.5835	0.114	0.0207	8.1364	4.4196
15	74.18	0.1051	+1.278	4.5967	0.114	0.0195	8.1604	4.4973
19	79.12	0.0907	+1.259	4.6306	0.114	0.0168	8.2131	4.6908
20	79.44	0.0910	+1.235	4.6323	0.114	0.0165	8.2021	4.7276
21	79.51	0.0913	+1.238	4.6314	0.114	0.0165	8.1945	4.7349
23	79.60	0.0919	+1.243	4.6292	0.114	0.0165	8.1819	4.7452
25	79.68	0.0928	+1.232	4.6284	0.114	0.0164	8.1698	4.7574
29	80.18	0.0970	+1.088	4.6332	0.114	0.0162	8.1230	4.8137
33	81.48	0.1000	+0.985	4.6368	0.115	0.0160	8.0820	4.8581
37	84.11	0.1011	+0.925	4.6403	0.125	0.0166	8.0725	4.8817
43	90.04	0.0990	+0.857	4.6517	0.144	0.0173	8.0848	4.9276
46	99.94	0.0985	+0.683	4.6704	0.173	0.0180	8.1013	5.0034
49	110.91	0.0986	+0.430	4.6954	0.210	0.0187	8.1187	5.1010
51	117.65	0.0990	+0.223	4.7151	0.237	0.0192	8.1313	5.1743
53	126.16	0.0984	-0.109	4.7497	0.282	0.0198	8.1590	5.2886
54	131.39	0.0996	-0.453	4.7814	0.318	0.0202	8.1724	5.3950

Table 8. The evolution of a helium star at 0.5 $M_\odot$; cf. Table 6.

model number	time in 10^6 years	events	increasing quantities	decreasing quantities	remarks
0	0.0000	A, a			
			L, R, T_c, ρ_c	T_e, $(He)_c$	T_e approximately constant
3	0.3693	B			
			L, R, T_e, T_c, ρ_c	$(He)_c$	mass in conv. core and T_e are approx. constant
8	0.6617	C			
			L, T_e, T_c, ρ_c	R, $(He)_c$	mass in conv. core and L are approx. constant
28	0.8482	d, e			
			L, T_e, T_c, ρ_c	R	
39	0.8553	f			
			L, T_e, T_c, ρ_c	R	convection zone appears at former core boundary
44	0.8562	D, E			
			L, R, T_c, ρ_c	T_e	
50	0.8599	H			

Table 9. Summary of the evolution of a helium star at 6 $M_\odot$; cf. Table 5.

model number	time in 10^6 years	$R/R_\odot$	M_{bol}	log T_e	$M_f/M_\odot$	$r_f/R_\odot$	log T_c	log ρ_c
0	0.0000	0.6445	- 6.897	5.0204	3.162	0.2248	8.2416	2.8956
1	0.1000	0.6640	- 6.955	5.0197	3.251	0.2284	8.2473	2.9023
2	0.2202	0.6874	- 7.024	5.0191	3.303	0.2299	8.2554	2.9148
3	0.3693	0.7153	- 7.109	5.0190	3.339	0.2292	8.2683	2.9397
5	0.5174	0.7367	- 7.193	5.0209	3.450	0.2296	8.2838	2.9724
8	0.6617	0.7494	- 7.280	5.0259	3.470	0.2213	8.3103	3.0391
11	0.7369	0.7409	- 7.330	5.0334	3.473	0.2117	8.3346	3.1056
14	0.7812	0.7204	- 7.365	5.0430	3.472	0.2013	8.3592	3.1758
19	0.8190	0.6734	- 7.409	5.0620	3.456	0.1829	8.4016	3.3006
24	0.8359	0.6216	- 7.448	5.0834	3.421	0.1642	8.4460	3.4333
28	0.8482	0.5741	- 7.478	5.1036	3.429	0.1497	8.4872	3.5567
32	0.8540	0.5507	- 7.508	5.1157	3.429	0.1406	8.5151	3.6427
39	0.8554	0.5384	- 7.537	5.1235	3.429	0.1338	8.5371	3.7232
42	0.8557	0.5360	- 7.545	5.1252	3.429	0.1320	8.5437	3.7493
44	0.8562	0.5352	- 7.550	5.1260	3.429	0.1303	8.5501	3.7754
47	0.8579	0.5542	- 7.574	5.1208	3.432	0.1269	8.5671	3.8567
48	0.8591	0.5821	- 7.617	5.1144	3.434	0.1250	8.5772	3.9203
50	0.8599	0.6059	- 7.653	5.1094	3.438	0.1233	8.5894	3.9675

Table 10. The evolution of a helium star at 6 $M_\odot$; cf. Table 6.

F_s	$F_{1/2}$	$F_{3/2}$	F_2	$F_{5/2}$	F_3
$\frac{s+1}{2}$	3/4	5/4	3/2	7/4	2
a_o	0.0000000	4.0444771	24.116961	57.584337	14.168719
a_1	0.0000000	8.6132186	13.082903	18.075336	17.573004
b_o	0.0000000	4.2063999	17.804124	28.101809	4.2945570
b_1	0.0000000	11.629816	21.782148	29.560025	8.7744807
b_2	1.5832098	7.0770719	8.7784752	10.160539	5.2799708

Table 11. Parameters for approximations of Fermi-Dirac functions. Each column corresponds to one Fermi-Dirac function; cf. equation A51.

reaction	$\frac{\text{number product nuclei formed}}{(\text{unit volume})(\text{unit time})}$	energy release per product nucleus formed
Helium burning		
$He^4(\alpha)Be^8(\alpha,\gamma)C^{12}$	$(x_\alpha)^3 R_{12}$	$Q_{12} = 7.282$ Mev $= 1.167 \times 10^{-5}$ erg
$C^{12}(\alpha,\gamma)O^{16}$	$(x_\alpha)(x_{12})R_{16}$	$Q_{16} = 7.162$ Mev $= 1.147 \times 10^{-5}$ erg
$O^{16}(\alpha,\gamma)Ne^{20}$	$(x_\alpha)(x_{16})R_{20}$	$Q_{20} = 4.730$ Mev $= 7.578 \times 10^{-6}$ erg
Carbon and Oxygen burning		
$C^{12}(C^{12},\gamma)Mg^{24}$	$(x_{12})^2 R_{24}$	$Q_{24} = 13.93$ Mev $= 2.232 \times 10^{-5}$ erg
$O^{16}(C^{12},\gamma)Si^{28}$	$(x_{12})(x_{16})R_{28}$	$Q_{28} = 16.75$ Mev $= 2.684 \times 10^{-5}$ erg
$O^{16}(O^{16},\gamma)S^{32}$	$(x_{16})^2 R_{32}$	$Q_{32} = 16.54$ Mev $= 2.650 \times 10^{-5}$ erg

Table 12. Summary of the nuclear reactions.
Each row corresponds to one reaction.

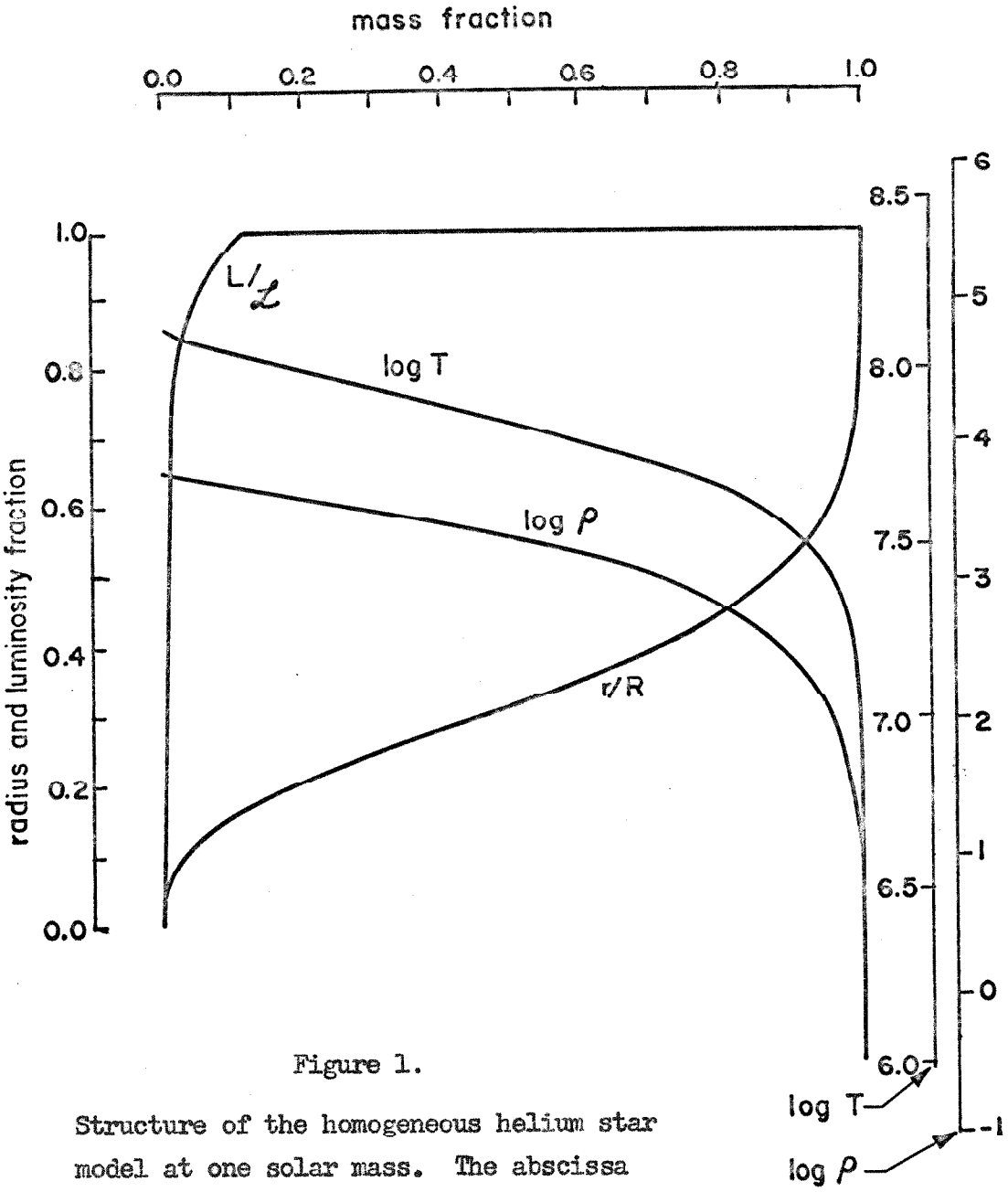

Figure 1.

Structure of the homogeneous helium star model at one solar mass. The abscissa represents the interior mass fraction, and the ordinate represents one of the quantities with which the four lines are labelled. The convective core extends to a mass fraction of 0.264.

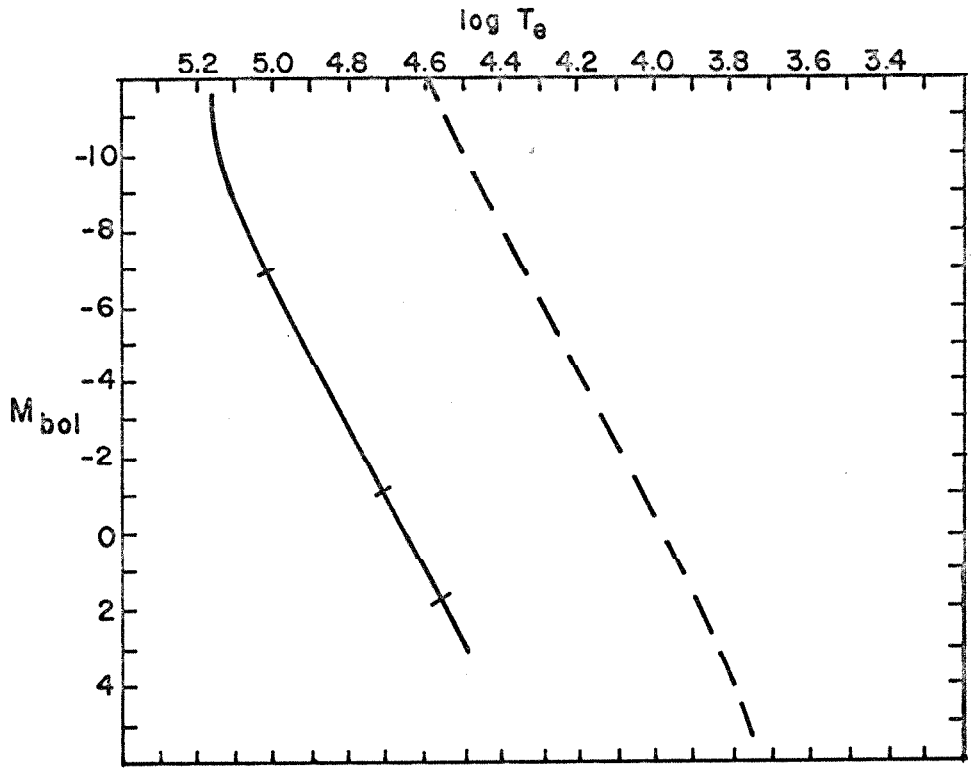

Figure 2.

Loci of models in the (M_{bol}, log T_e) plane. The solid line represents the homogeneous helium star models of the present study, and the dashed line represents the normal dwarf (hydrogen star) main sequence, taken from Allen (1963).

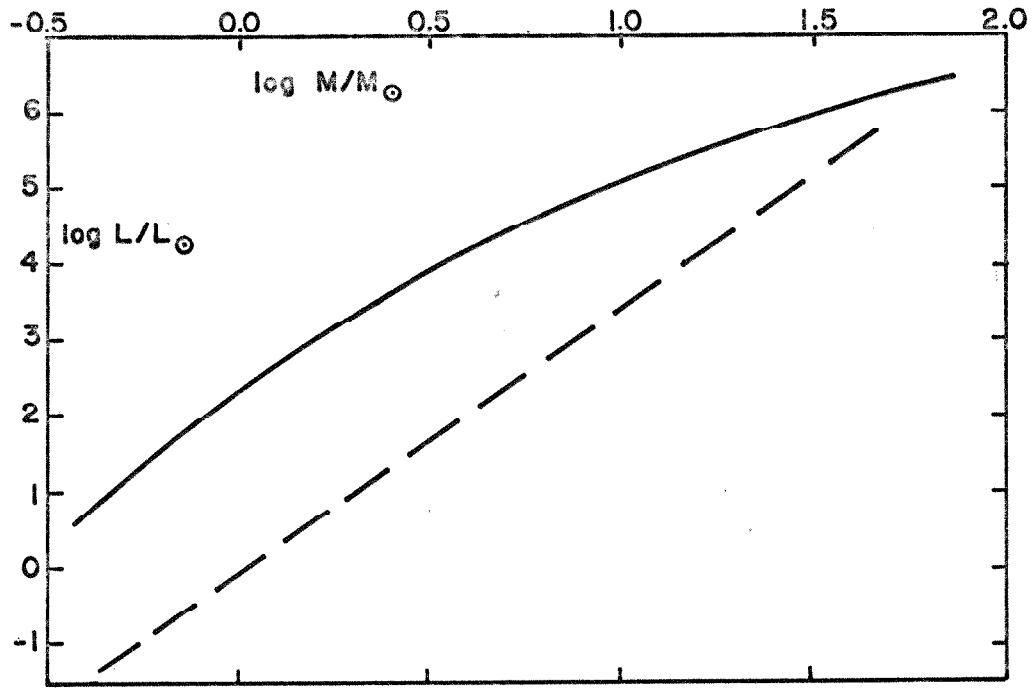

Figure 3.

The mass luminosity relation for the homogeneous helium star models of the present study (solid line) and for the normal dwarf main sequence (dashed line; values taken from Allen (1963)).

Figure 4. (Drawing on page 98).

Nuclear abundances in the evolution of a helium star at one solar mass. The abscissa represents time and the ordinate represents the fraction by mass of the various species. Subscripts c indicate values at the center of the star and subscripts av indicate the average composition of the star. Until a time of 12.2×10^6 years the central values apply to the entire convective core (mass fraction 0.267); thereafter they are constant with time. Not all of the average composition curves are shown in the early evolutionary stages.

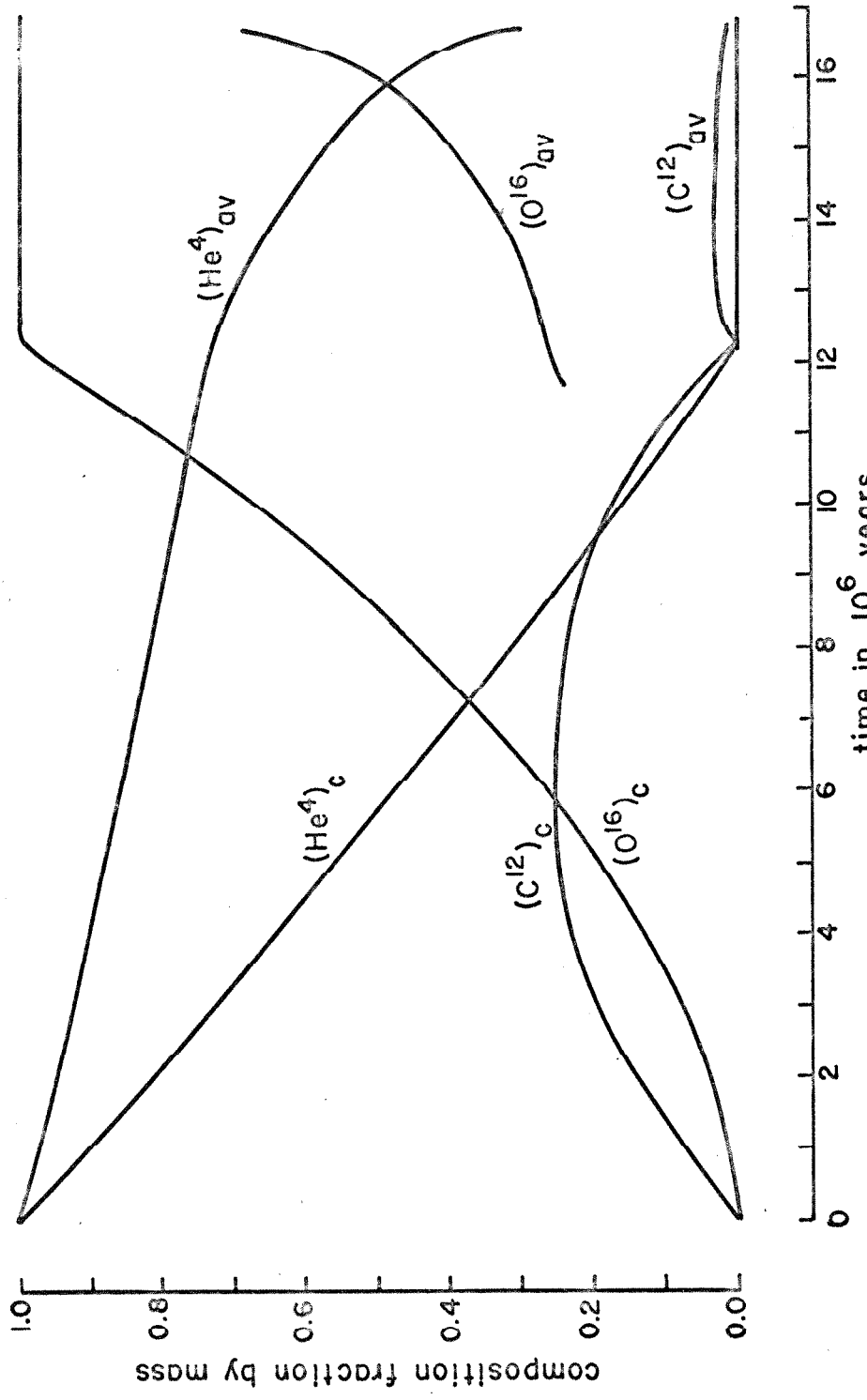

Figure 4. (Caption on page 97).

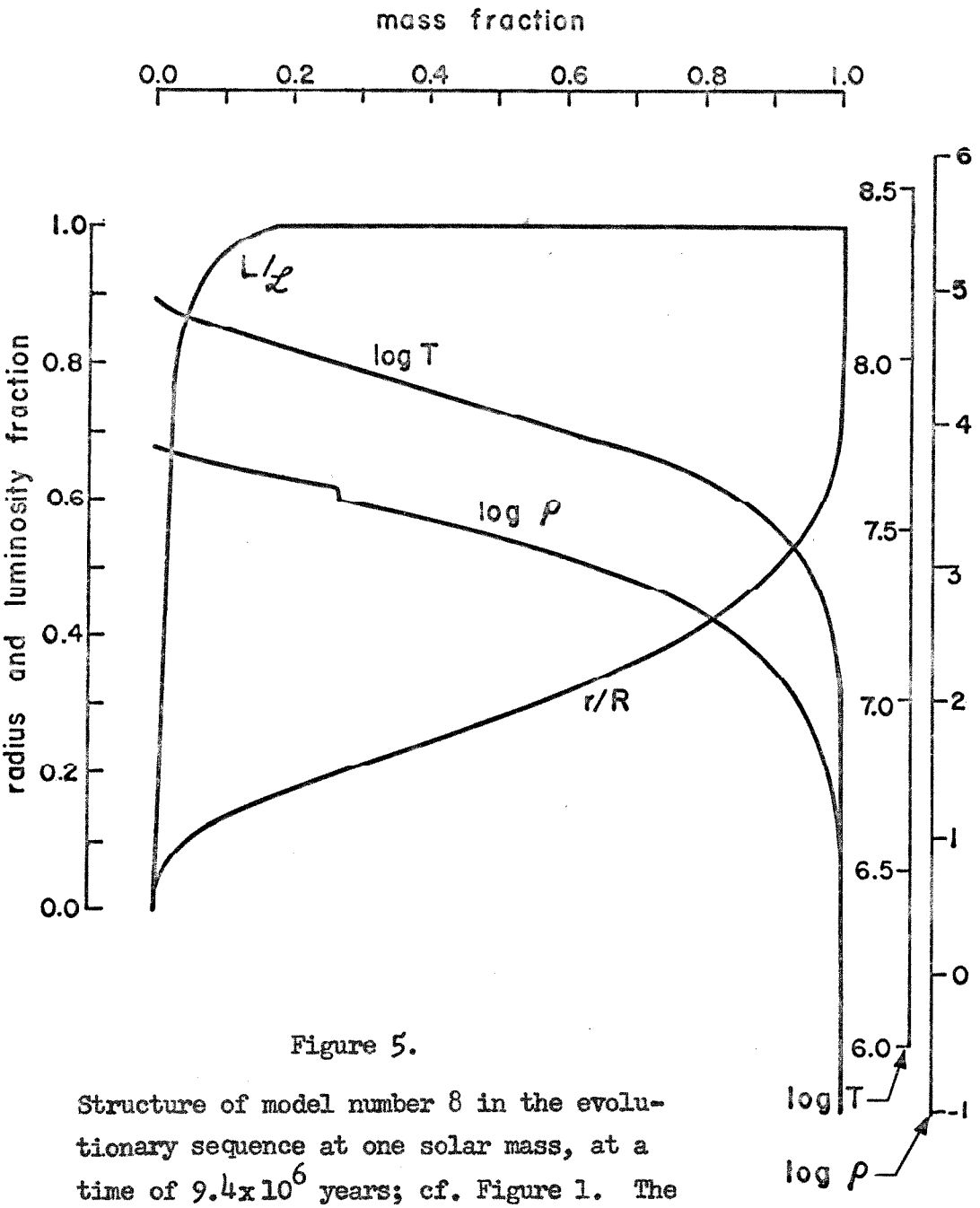

Figure 5.

Structure of model number 8 in the evolutionary sequence at one solar mass, at a time of 9.4×10^6 years; cf. Figure 1. The discontinuity in log ρ occurs at the edge of the convective core, at mass fraction 0.267.

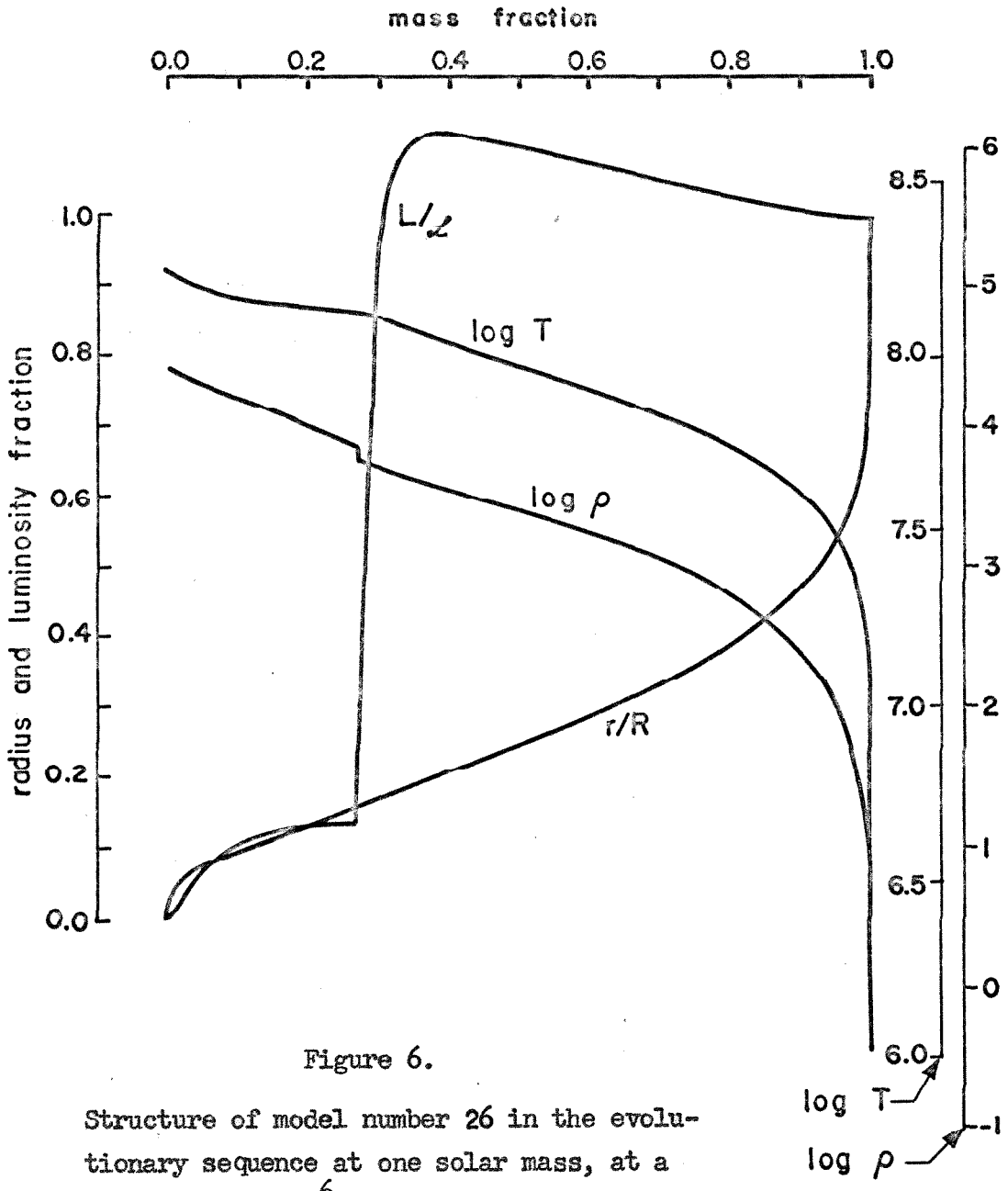

Figure 6.

Structure of model number 26 in the evolutionary sequence at one solar mass, at a time of 12.3×10^6 years; cf. Figure 1. The shell source at the former convective core boundary is distinguished by a discontinuity in $\log \rho$ and by a sharp rise in the luminosity.

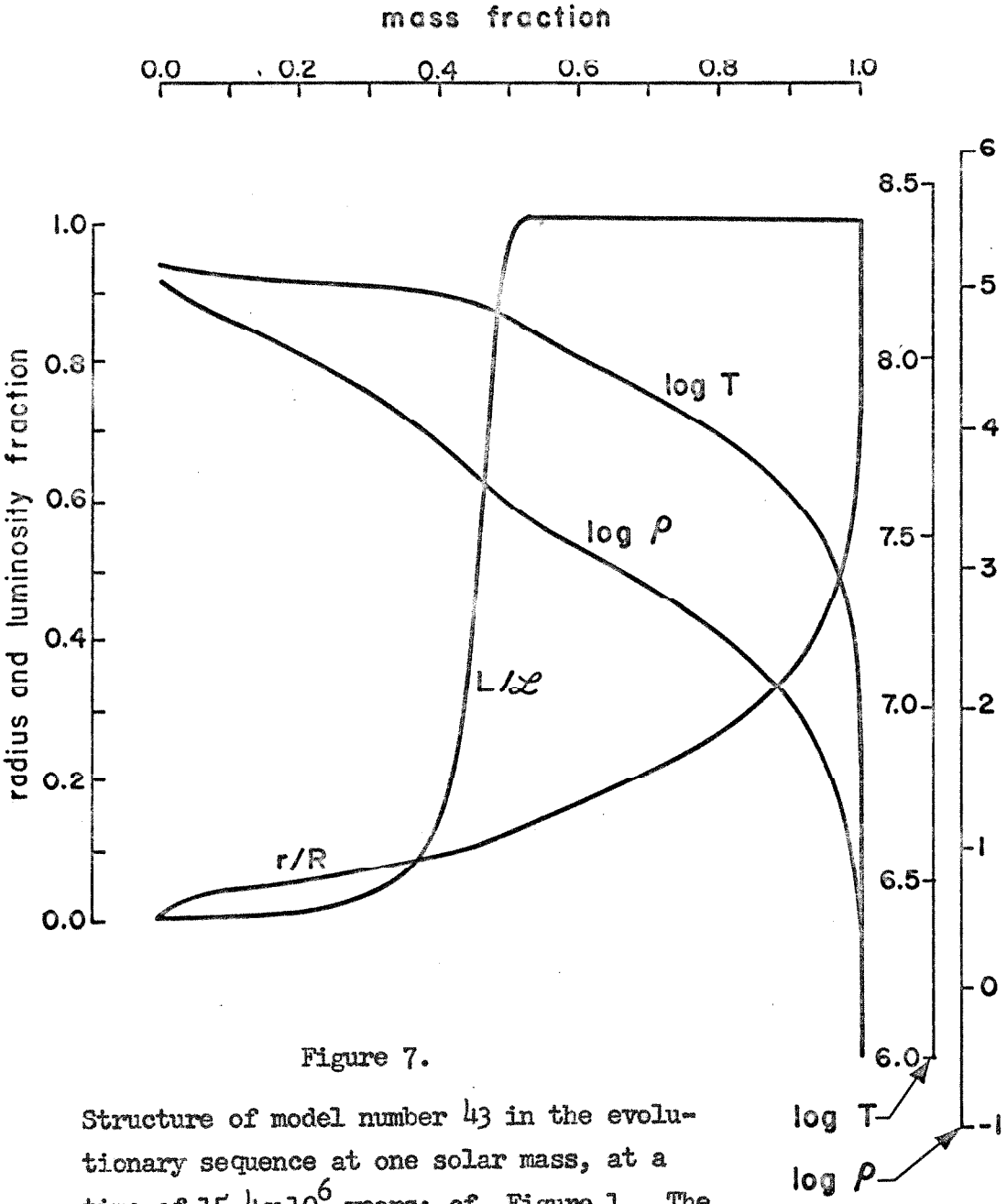

Figure 7.

Structure of model number 43 in the evolutionary sequence at one solar mass, at a time of 15.4×10^6 years; cf. Figure 1. The shell source has moved out to a mass fraction of 0.464.

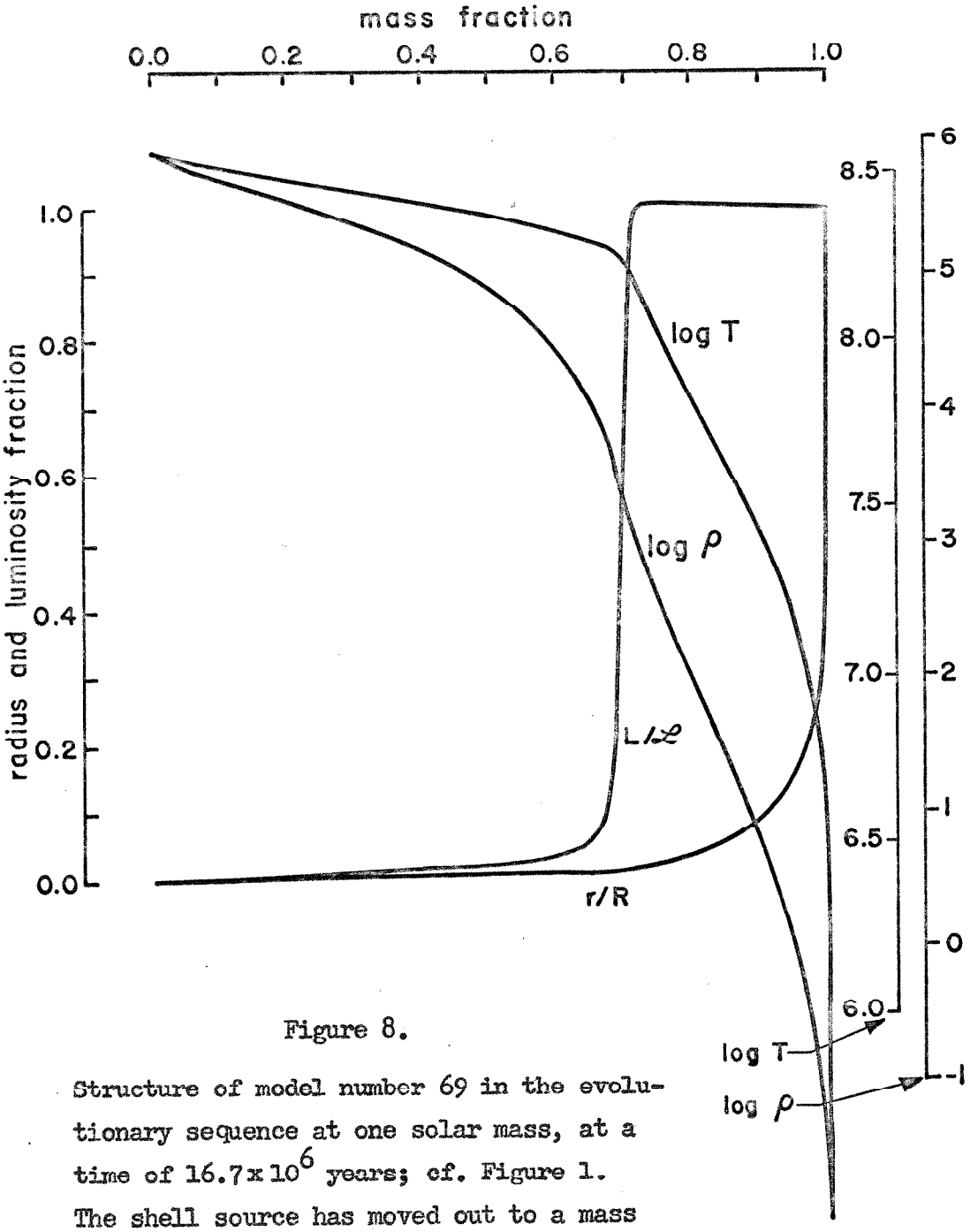

Figure 8.

Structure of model number 69 in the evolutionary sequence at one solar mass, at a time of 16.7×10^6 years; cf. Figure 1. The shell source has moved out to a mass fraction of 0.701.

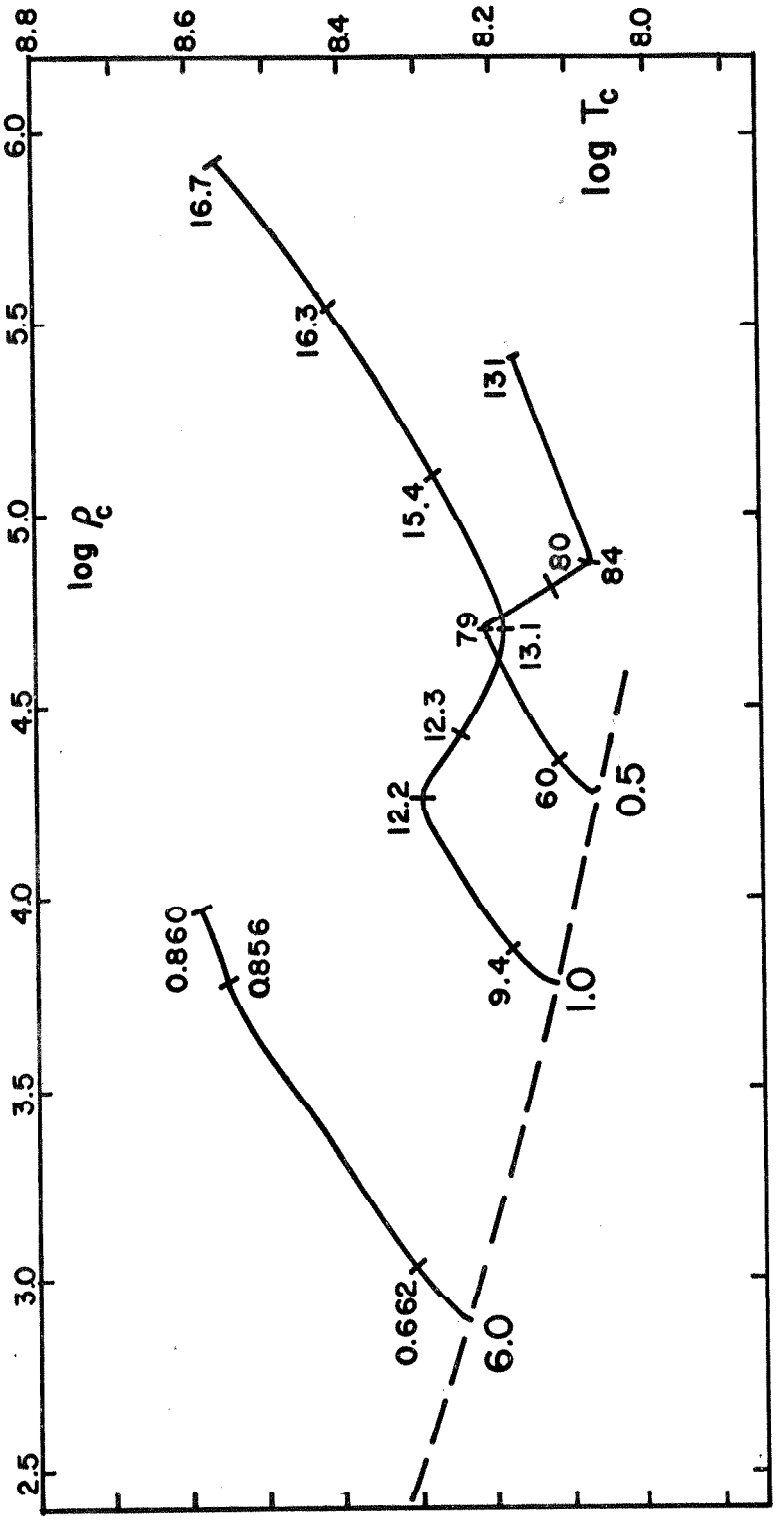

Figure 9. Loci of model centers in the ($\log T$, $\log \rho$) plane. The dashed line represents the main sequence of homogeneous helium star models. The solid lines represent the tracks of evolving helium star models, for which the large numbers indicate the model masses (0.5, 1.0, and 6.0) in solar units and the small numbers indicate evolutionary times (beyond the main sequence position) in millions of years.

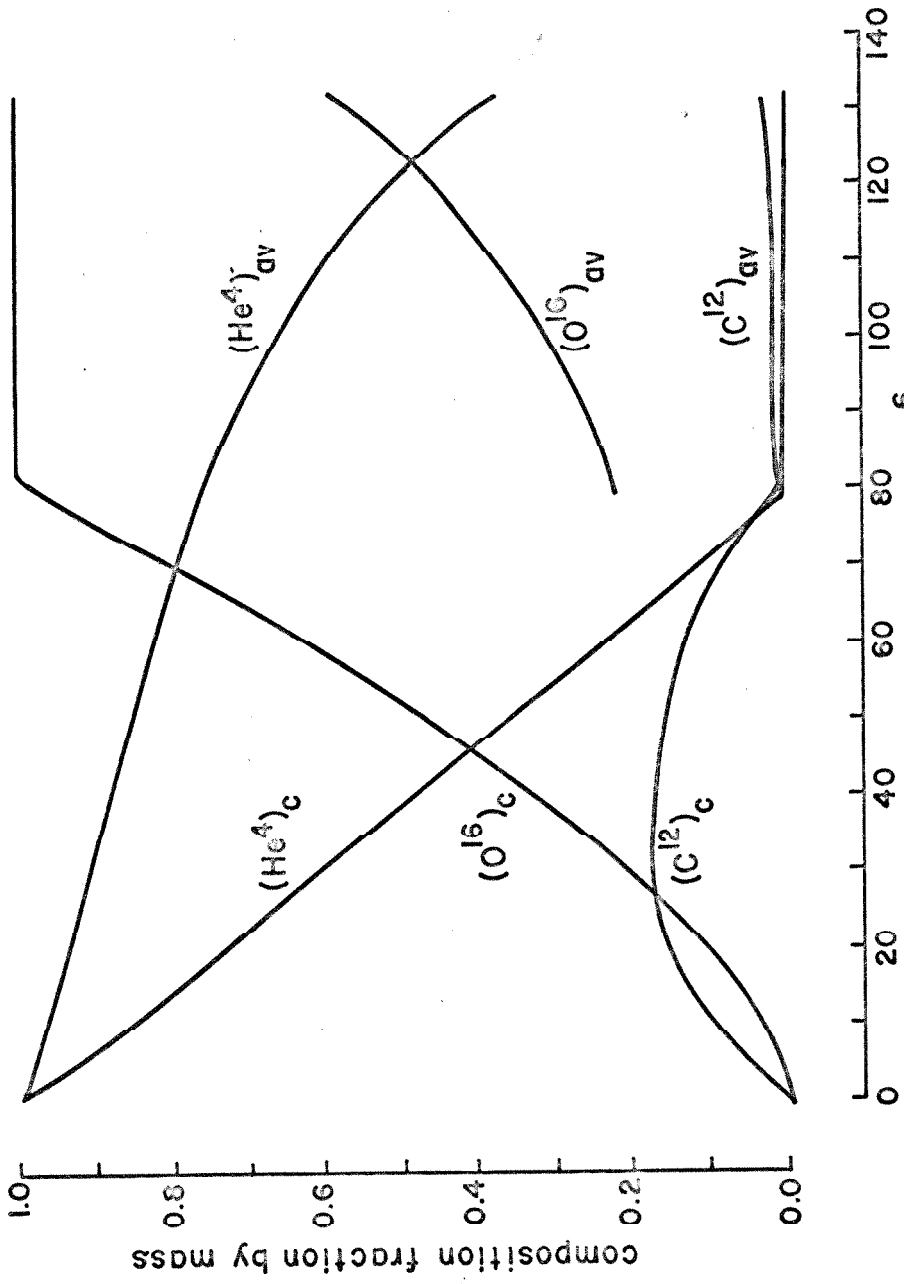

Figure 10. Nuclear abundances in the evolution of a helium star at 0.5 $M_\odot$; cf. Figure 4.

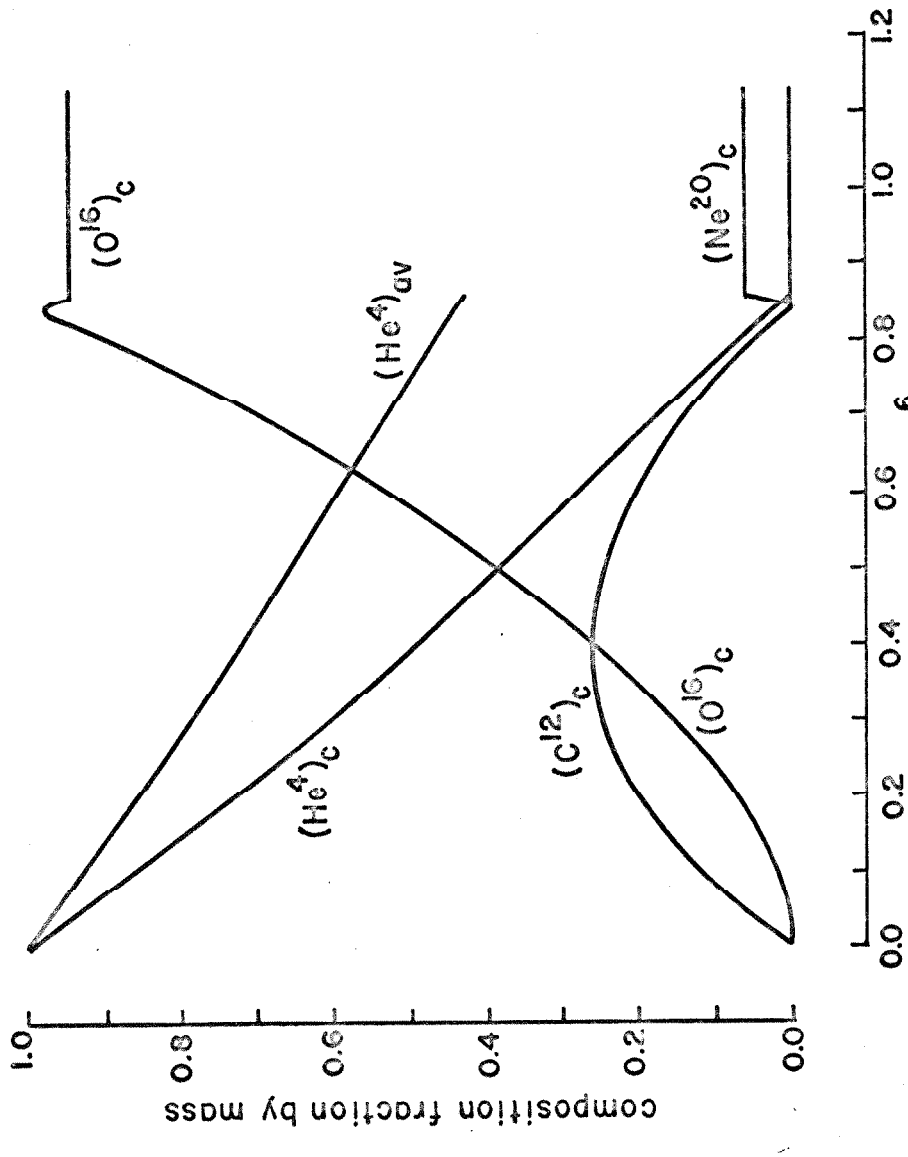

Figure 11. Nuclear abundances in the evolution of a helium star at 6 $M_\odot$; cf. Figure 4.

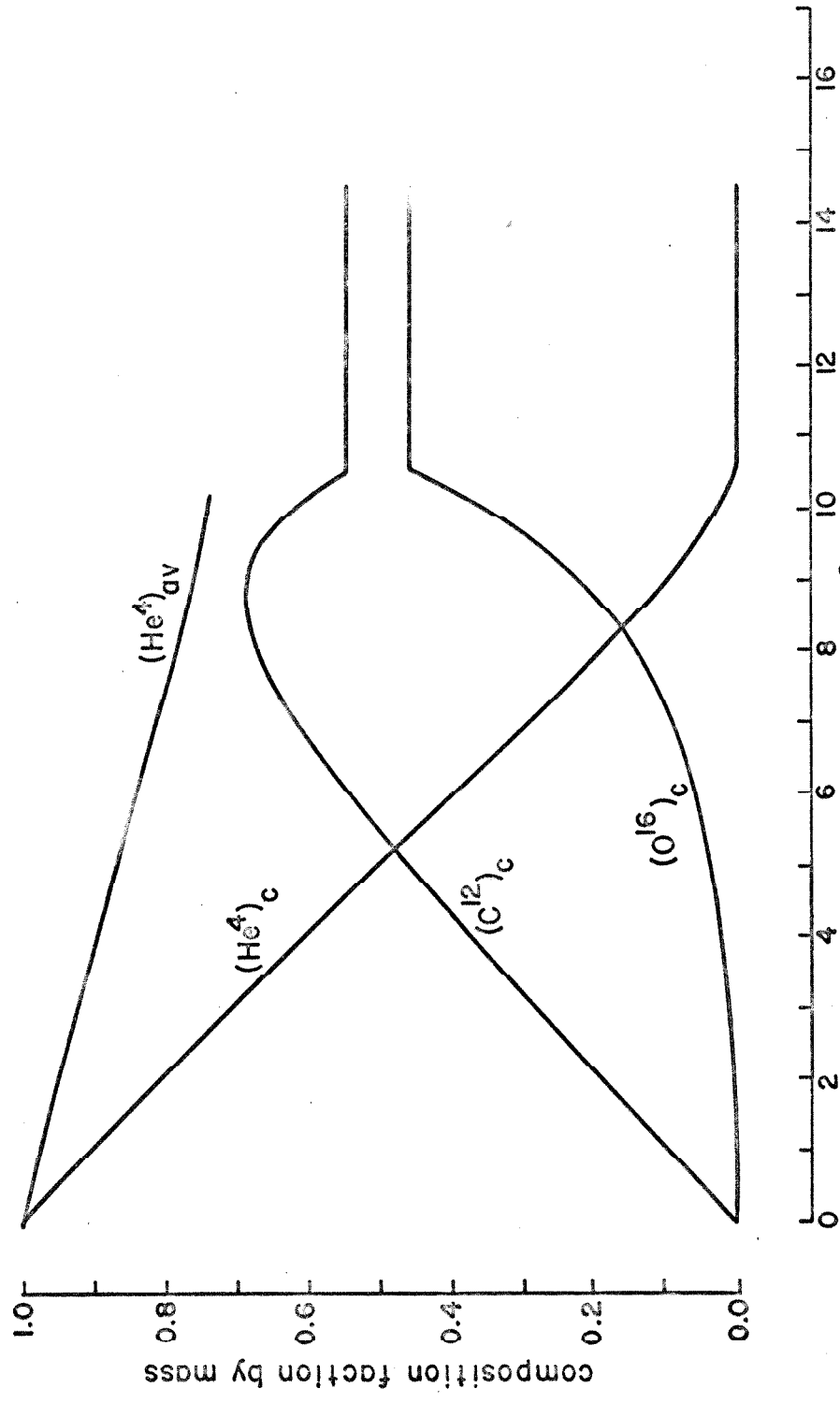

Figure 12. Nuclear abundances in the evolution of a helium star at one solar mass using a reaction rate for $C^{12}(\alpha,\gamma)O^{16}$ reduced by a factor ten; cf. Figure 4.

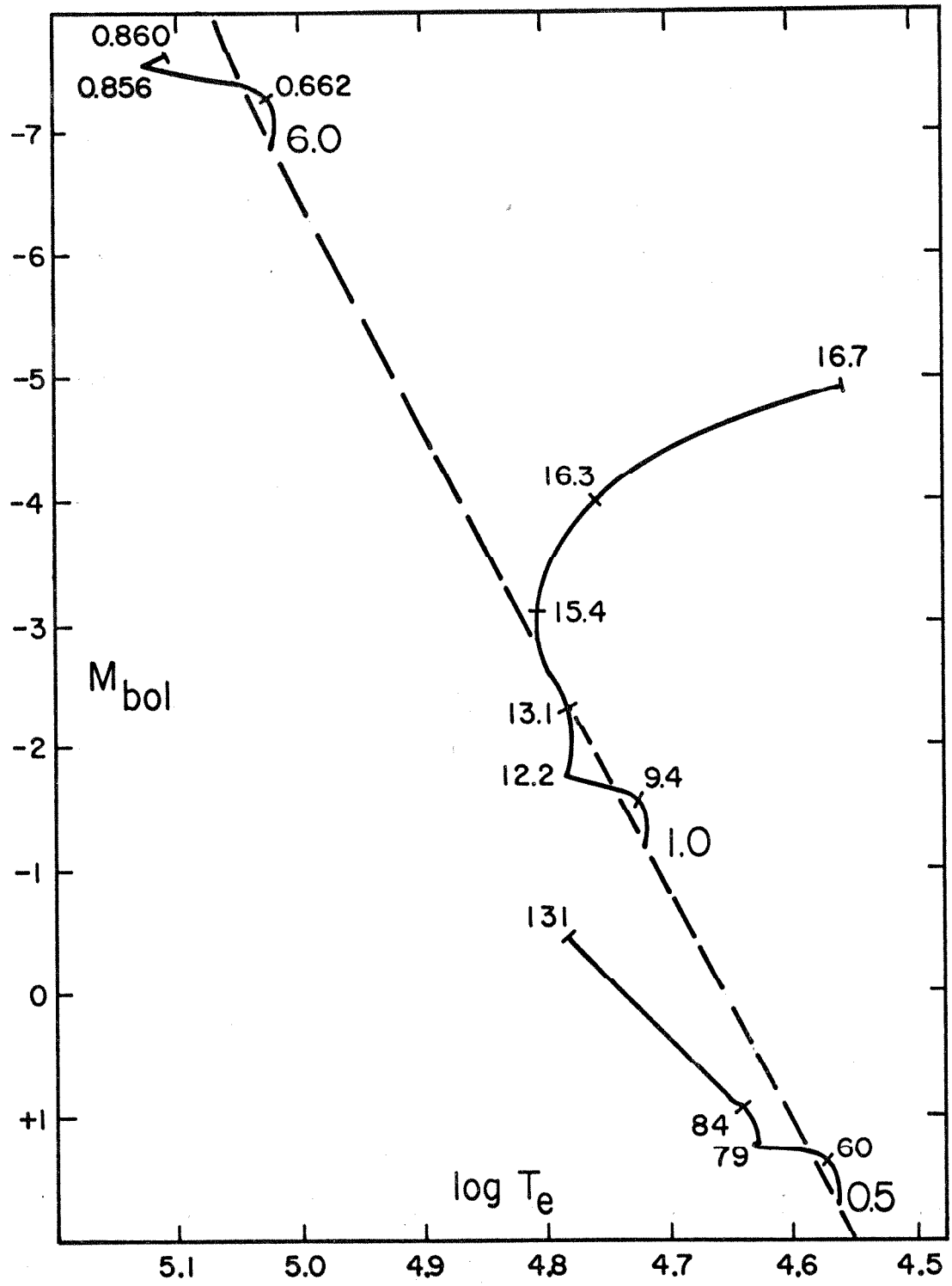

Figure 13. (Caption on page 109).

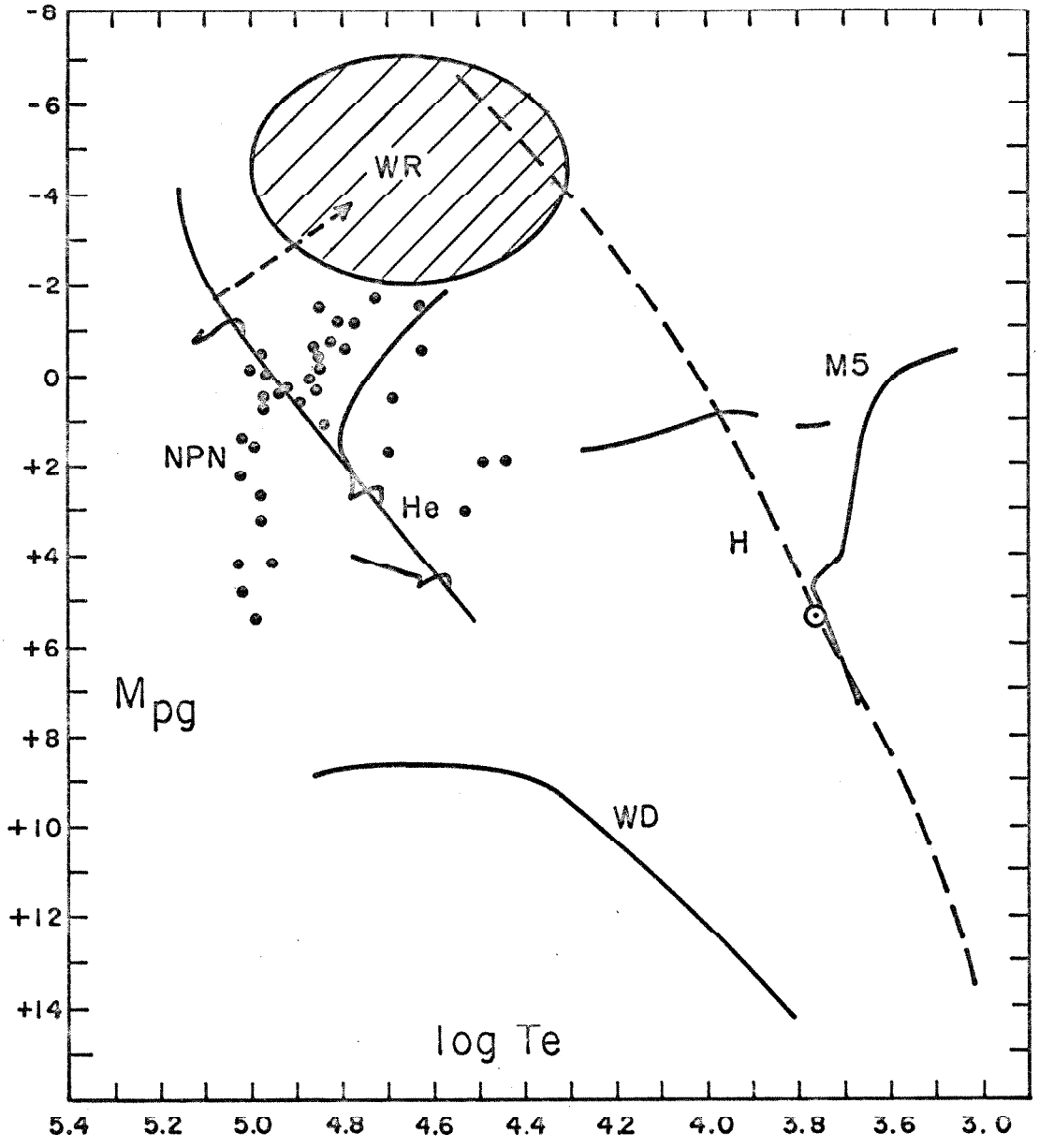

Figure 14. (Caption on page 109).

Figure 13.

Loci of helium star models in the (M_{bol}, log T_e) plane. The dashed line represents the main sequence of homogeneous helium star models. The solid lines represent the tracks of evolving helium star models, for which the large numbers indicate the model masses (0.5, 1.0, and 6.0) in solar units and the small numbers indicate evolutionary times (beyond the main sequence position) in millions of years.

Figure 14.

The (M_{pg}, log T_e) plane. The various labelled entries are as follows:

H The normal dwarf (hydrogen star) main sequence, including the sun (⊙).

He The helium star models of the present study, including the main sequence and three evolutionary tracks; the effect of a hydrogen-rich shell on the model at 10 $M_\odot$ is indicated by a dashed arrow.

M5 Locus of normal points for the globular cluster M5.

NPN The region of the nuclei of planetary nebulae, for which the dots indicate individual stars.

WD Line of the white dwarf stars.

WR Region somewhere within which the Wolf-Rayet stars may be located.

The sources of data for these entries are noted in the text of Section IV-2.

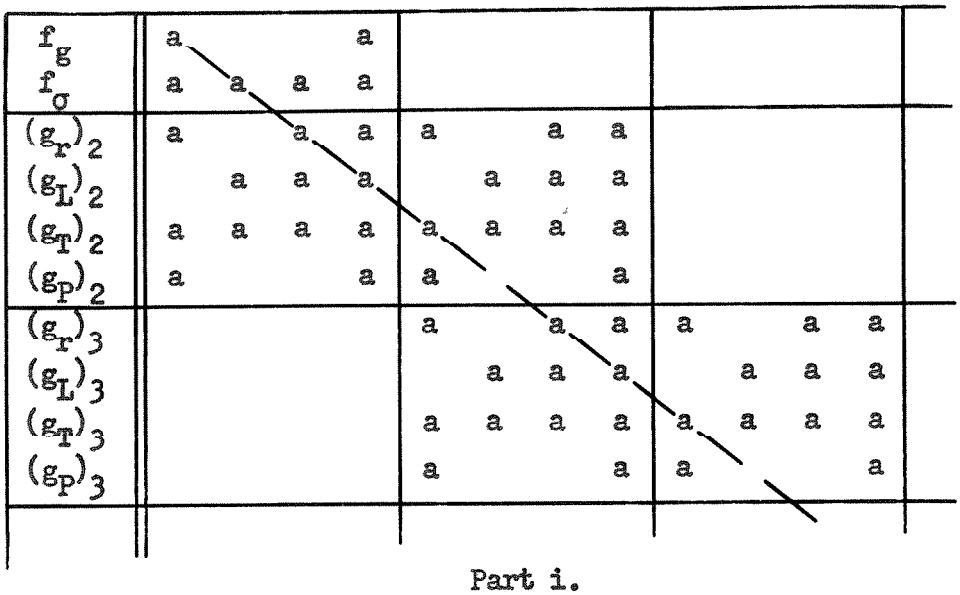

Part i.

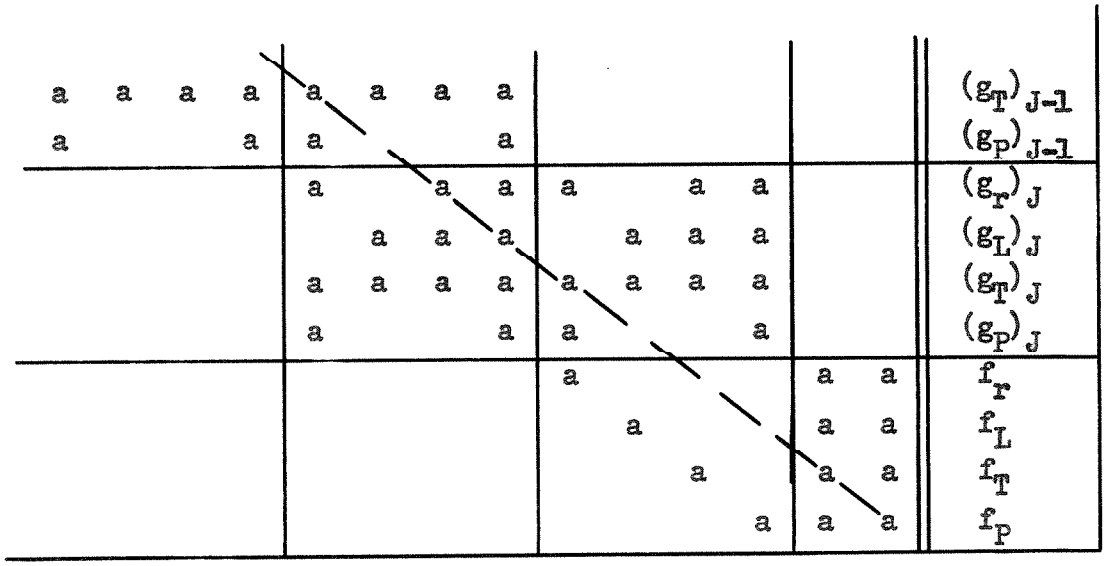

Part ii.

Figure 15. (Caption on page 111).

Figure 15.

Elements of the matrix $\underset{\sim}{A}$.

Part i. Upper left corner (surface).

Part ii. Lower right corner (center).

The columns correspond to the unknown elements of the vector $\underset{\sim}{x}$ (cf. form B36); the rows correspond to the several equations of the system B38, as indicated (here JAY is shortened to J). An entry a indicates a non-zero element and a blank indicates a zero element; those along the diagonal are connected by a dashed line.